Involvement of AAA ATPase AipA in endocytosis of the arginine permease AoCan1 depending on AoAbp1 in Aspergillus oryzae

Hiasa, Reiko
Department of Bioscience and Biotechnology, Faculty of Agriculture, Kyushu University

Kakimoto, Ken-ichi
Department of Bioscience and Biotechnology, Faculty of Agriculture, Kyushu University

Takegawa, Kaoru
Department of Bioscience and Biotechnology, Faculty of Agriculture, Kyushu University

Higuchi, Yujiro
Department of Bioscience and Biotechnology, Faculty of Agriculture, Kyushu University

出版情報：Fungal Biology. 126 (2), pp.149-161, 2022-02. Elsevier
バージョン：
権利関係：

Involvement of AAA ATPase AipA in endocytosis of the arginine permease AoCan1 depending on AoAbp1 in *Aspergillus oryzae*

Reiko Hiasa, Ken-ichi Kakimoto, Kaoru Takegawa, Yujiro Higuchi*

Department of Bioscience and Biotechnology, Faculty of Agriculture, Kyushu University, 744 Motooka, Fukuoka 819-0395, Japan

*Corresponding author. Tel/Fax: +81 92 802 4734, E-mail address: y.higuchi@agr.kyushu-u.ac.jp

Word count: Abstract, 250; Main, 5519.

Number of figures: Main, 9; Supplementary, 5.

Number of tables: Main, 2.

Abstract

AAA (ATPases associated with diverse cellular activities) ATPases widely exist in many organisms and function in various organelles. However, there is little information about AAA ATPase functioning in endocytosis. In the filamentous fungus *Aspergillus oryzae*, we previously discovered a putative AAA ATPase AipA (AoAbp1 interacting protein) that would be involved in endocytosis. Here, we further examined the function of AipA and AoAbp1 in endocytosis using enhanced green fluorescent protein (EGFP)-tagged arginine permease AoCan1 as an endocytic marker. In the Δ*aipA* strain, endocytosis of AoCan1-EGFP was more facilitated than the control strain, suggesting that AipA negatively regulates endocytosis. Additionally, the localization of F-actin, visualized by Lifeact-EGFP, was concentrated at the hyphal tip in the Δ*aipA* strain than the control strain, suggesting that endocytosis was promoted due to enhanced actin polymerization in the Δ*aipA* strain. In contrast, in the Δ*Aoabp1* strain, endocytosis of AoCan1-EGFP was delayed compared with the control strain, suggesting that AoAbp1 positively functions in endocytosis. In addition, in the Δ*aipA*Δ*Aoabp1* strain, endocytosis of AoCan1-EGFP was also delayed. AipA localized at the endocytic collar of the hyphal tip, only in the presence of AoAbp1, suggesting that AipA functions downstream of AoAbp1 in endocytosis. Moreover, we investigated the *aipA*-

overexpressing strain, and found that endocytosis of AoCan1-EGFP was inhibited. Furthermore, we examined strains expressing *aipA*^{K542A} or *aipA*^{E596Q}, which decreased ATPase activity, in the backgrounds of complementation or overexpression, respectively, and found that AoCan1-EGFP endocytosis was promoted. These results suggested that AAA ATPase activity of AipA is important for its function in endocytosis.

Keywords: AAA ATPase; AipA; AoAbp1; *Aspergillus oryzae*; endocytosis

Introduction

Intracellular trafficking is a vesicle-mediated transport pathway for substances between eukaryotic organelles. Membrane proteins and extracellular substances are taken up by endocytosis via vesicles produced by the plasma membrane and transported to early endosomes. Early endosomes then mature to late endosomes, and substances to be degraded are transported from late endosomes to lysosomes/vacuoles. On the other hand, substances to be recycled are transported from early endosomes to the Golgi apparatus and then transported to the plasma membrane or directly from early endosomes to the plasma membrane. Endocytosis is an essential intracellular machinery highly conserved in eukaryotic cells that is involved in numerous processes, such as the acquisition of nutrients and signal transduction (Polo & Di, 2006). Detailed molecular mechanisms of endocytosis have been studied in the model yeast *Saccharomyces cerevisiae* and mammalian cells, and there are at least 10 estimated modes of endocytosis (McDermott & Kim, 2015). In particular, clathrin-mediated endocytosis (CME) is well studied, and in *S. cerevisiae*, CME occurs near actin-rich cell membranes called actin patches (Kim *et al*. 2006).

Filamentous fungi also have the process of endocytosis but its molecular machinery has not yet been clarified well compared with yeasts (Peñalva 2010). In a model

filamentous fungus *Aspergillus nidulans*, endocytosis was studied by using a lipophilic dye FM4-64 that is non-selectively incorporated from the plasma membrane (Peñalva 2005). In addition, in another model filamentous fungus *Aspergillus oryzae*, endocytosis was studied by fusing the plasma membrane proteins AoUapC (uric acid-xanthine permease), arginine permease AoCan1 (canavanine resistance), and maltose transporter MalP (maltose permease) with enhanced green fluorescent protein (EGFP), as marker proteins for endocytosis (Higuchi *et al*. 2006; Matsuo *et al*. 2013; Hiramoto *et al*. 2015). In *S. cerevisiae*, Can1 is a member of MCC (membrane compartment of Can1p) compartments and endocytosis of Can1-GFP is severely inhibited in the *sla2*/*end4* mutant (Grossmann *et al*. 2008). It has become possible to analyze endocytosis in various filamentous fungi, which clarified that endocytosis actively occurs at a site called the endocytic collar, membrane regions slightly away from the hyphal tip. For example, in *A. nidulans*, localization analyses of AbpA, SlaB, FimA corresponding to Abp1, End4/Sla2, Sac6 of *S. cerevisiae*, respectively, revealed that these proteins mostly localize at the endocytic collar (Araujo-Bazán *et al*. 2008; Taheri-Talesh *et al*. 2008; Upadhyay & Shaw 2008), similar results of which were also seen in a model filamentous fungus *Neurospora crassa* (Echauri-Espinosa *et al*. 2012; Lara-Rojas *et al*. 2016; Bartnicki-Garcia *et al*. 2018). Substances taken up by endocytosis

from the endocytic collar are thought to include *A. nidulans* SynA and *A. oryzae* AoSnc1, a SNARE (soluble *N*-ethylmaleimide-sensitive factor attachment protein receptor) protein, a flippase DnfA, and coronin involved in the formation of actin patches in *N. crassa*. These proteins have been shown to be endocytosed from the plasma membrane and recycled to the hyphal tip (Higuchi *et al*. 2009a; Pantazopoulou & Peñalva 2011; Shaw *et al*. 2011; Echauri-Espinosa *et al*. 2012; Schultzhaus *et al*. 2015).

A. oryzae has been used in the industrial fermentation and can secrete a large amount of useful enzymes, such as amylases. In *A. oryzae* intracellular transport pathway, it has been thought that secretory pathway and endocytosis are linked through the apical endocytic recycling (Higuchi *et al*. 2009b; Shoji *et al*. 2014; Higuchi, 2021a; Higuchi, 2021b). In a previous study, we discovered a putative AAA (ATPase associated with diverse cellular activities) ATPase AipA (AoAbp1 interacting protein) as a binding partner of AoAbp1 by a yeast two-hybrid screening (Higuchi *et al*. 2011). AAA ATPase family proteins have one or two highly conserved AAA ATPase domains at the C-terminal region, by which ring-shaped hexamer is formed to generally function in dissociation of protein complexes and membrane fusion (White & Lauring 2007). In an *aipA*-overexpressing strain, both growth and endocytic recycling of FM4-64 to the

apical vesicle cluster Spitzenkörper (Spk) were delayed, suggesting that AipA has a negative function at the apical region of hyphae in growth and endocytosis (Higuchi *et al*. 2011). In this study, we further investigated the function of AipA and AoAbp1 in endocytosis of AoCan1 and their functional dependency. We revealed that AipA negatively and AoAbp1 positively control endocytosis of AoCan1, in which AipA functions downstream of AoAbp1.

Materials and methods

Strains and media of A. oryzae

All *A. oryzae* strains used in this study are listed in Table 1. The genomic DNA of the wild-type (WT) *A. oryzae* strain RIB40 was used for general DNA cloning.

Czapek-Dox (CD) medium (0.3% $NaNO_3$, 0.2% KCl, 0.1% KH_2PO_4, 0.05% $MgSO_4 \cdot 7H_2O$, 0.002% $FeSO_4 \cdot 7H_2O$ and 2% glucose, pH 5.5) and Minimal (M) medium (0.2% NH_4Cl, 0.1% $(NH_4)_2SO_4$, 0.05% KCl, 0.05% NaCl, 0.1% KH_2PO_4, 0.05% $MgSO_4 \cdot 7H_2O$, 0.002% $FeSO_4 \cdot 7H_2O$ and 2% glucose, pH 5.5) were used as standard media. For strain auxotrophy, 0.0015% methionine was added to CD medium (CDm). When indicated, glucose was replaced with maltose (CDm-mal), 5 mM L-arginine was added to CD or CDm medium (CD+arg or CDm+arg), 75 nM itraconazole (ITA), and 6 mM H_2O_2. For rich growth cultures, potato dextrose (PD, Nissui) was used. Approximately 10^3 or 10^5 conidia of each strain were inoculated on each plate and subsequently cultured at 30°C or 37°C for several days.

Construction of plasmids and strains

To construct control strains, we used expression vectors pgniaD carrying the sequence of *niaD* selective marker, pgNotI-AosC and pgNotI-AosC-NotI carrying the

sequence of *AosC* selective marker, and pgSmaI-ptrA-SmaI carrying the sequence of *ptrA* selective marker (Togo *et al*. 2017). pgniaD, pgNotI-AosC, pgNotI-AosC-NotI and pgSmaI-ptrA-SmaI were introduced into each strain DAIPA1, NSRku70-1-1AN and DAIPA1-N, DAIPA1-N-Can1E and DABP1-Can1E, respectively, by *A. oryzae* transformation.

To construct Δ*Aoabp1* and Δ*aipA*Δ*Aoabp1* strains, we used pgNotI-AosC-NotI. Approximately 1 kb each of the upstream and downstream region of *Aoabp1* ORF was amplified by PCR using PrimeSTAR GXL DNA polymerase (Takara) and the primer sets KK260 and KK261, and KK262 and KK263, respectively. pgNotI-AosC-NotI was digested by NotI and ligated with the PCR-amplified sequences by In-Fusion reaction (Takara), resulting in pgΔAoabp1. The DNA fragment for deletion of *Aoabp1* was obtained by digesting pgΔAoabp1 with NotI, and then introduced into the *Aoabp1* locus in strains NSRku70-1-1A and DAIPAS1 (Δ*aipA*) by *A. oryzae* transformation.

To construct strains endogenously expressing AoCan1 C-terminally fused with EGFP, we used the expression vector pgSmaI-egfp-TamyB-ptrA-SmaI carrying the sequence of *egfp*, T*amyB* and the *ptrA* marker. Approximately 1 kb each of the ORF and downstream region of *Aocan1* was amplified by PCR using PrimeSTAR GXL DNA polymerase and the primer sets KK312 and KK313, and KK314 and KK315,

136 respectively. pgSmaI-egfp-TamyB-ptrA-SmaI was digested by SmaI and ligated with
137 the PCR-amplified sequences by In-Fusion reaction, resulting in pgAocan1-*egfp*-IL-
138 *ptrA*. For exchanging the marker *ptrA* to *niaD*, *niaD* and the other plasmid sequences
139 were amplified by PCR using KOD FX DNA polymerase (TOYOBO) and the primer
140 sets YM16 and YM17, and SH21 and SH22, respectively. The *Aocan1-egfp-ptrA* or
141 *Aocan1-egfp-niaD* sequence was obtained by digesting with SmaI, and then introduced
142 into the *Aocan1* locus in strains DAIPA-com, PaaA1, PaaA5421, PaaA5961, NSRku70-
143 1-1ANSO, DAIPA1-NS, DAIPA1-N, NSRku70-1-1AS, DABP1 and DAIPAABP1 by *A.*
144 *oryzae* transformation.
145 To construct complementary strains of *aipA*, we used pgNotI-AosC-NotI. The DNA
146 sequences of *AosC* and the other plasmid sequence was amplified by inverse PCR
147 using PrimeSTAR GXL DNA polymerase and the primer set KK134 and YM83.The
148 DNA sequences of P*aipA*, *aipA* ORF, and T*aipA* were amplified by PCR using
149 PrimeSTAR GXL DNA polymerase and the primer set RH169 and RH170, and ligated
150 with the PCR-amplified sequence by In-Fusion reaction, resulting in pgPaipA-aipA-
151 TaipA. The mutant $aipA^{K542A}$ and $aipA^{E596Q}$ expressing vector was amplified by PCR
152 using PrimeSTAR Max DNA polymerase (Takara) and the primer sets RH150 and
153 RH151, and RH152 and RH153, respectively, and ligated with the PCR-amplified

154 sequences by In-Fusion reaction, resulting in pgPaipA-aipA^{K542A}-TaipA and pgPaipA-
155 aipA^{E596Q}-TaipA. These plasmids were introduced into the strain DAIPA1-N-Can1E by
156 *A. oryzae* transformation.
157 To construct a complementary strain of *Aoabp1*, we used pgSmaI-ptrA-SmaI. The
158 DNA sequence of *ptrA* and the other plasmid sequence were amplified by inverse PCR
159 using PrimeSTAR GXL DNA polymerase and the primer set KK217 and KK305. The
160 DNA sequences of P*Aoabp1*, *Aoabp1* ORF, and T*Aoabp1* were amplified by PCR using
161 PrimeSTAR GXL DNA polymerase and the primer set RH173 and RH174. This plasmid
162 was introduced into the DABP1-Can1E by *A. oryzae* transformation.
163 To construct strains expressing Lifeact C-terminally fused with EGFP, we used the
164 expression vector pgPamyB-SmaI-egfp-TamyB carrying the sequence of *egfp*, T*amyB*
165 and the *niaD* marker. The DNA sequence of *lifeact* was amplified by inverse PCR using
166 PrimeSTAR GXL DNA polymerase and the primer set YHK251 and YHK252, and
167 ligated with the PCR-amplified sequence by In-Fusion reaction, resulting in pgPamyB-
168 lifeact-egfp-niaD. Then, the P*amyB* was replaced with the promoter of *pgkA* (P*pgkA*) by
169 the same method using the primer sets YM56 and RH161, and RH160 and YM60,
170 resulting in pgPpgkA-lifeact-egfp-niaD. This plasmid was introduced into the NSRku70-
171 1-1AS, DAIPAS1, DABP1, and DAIPAABP1 by *A. oryzae* transformation.

To construct strains expressing AipA N-terminally fused with EGFP, we used the expression vector pgPamyB-mdsred-aipA-TamyB carrying the sequence of P*amyB*, aipA, T*amyB*, and the *niaD* marker. The DNA sequence of *egfp* and the other plasmid sequence were amplified by PCR using PrimeSTAR MAX DNA polymerase and the primer sets KK346 and KK347, and KK348 and KK349, respectively, and ligated with the PCR-amplified sequence by In-Fusion reaction, resulting in pgPamyB-egfp-aipA-TamyB. This plasmid was introduced into strains DAIPAS1 and DAIPAABP1 by *A. oryzae* transformation. Then, to construct strains expressing mutant AipA N-terminally fused with EGFP, the DNA sequences of $aipA^{K542A}$, $aipA^{E596Q}$ or $aipA^{\Delta 346\text{-}370}$ and the other plasmid sequence were amplified by inverse PCR using PrimeSTAR GXL DNA polymerase and the primer sets RH150 and RH151, and RH171 and RH172, respectively, and ligated with the PCR-amplified sequence by In-Fusion reaction, resulting in pgPamyB-egfp-aipA^{K542A}/aipA^{E596Q}/aipA$^{\Delta 346\text{-}370}$-TamyB. These plasmids were introduced into the strain DAIPAS1 by *A. oryzae* transformation.

To construct strains expressing AoAbp1 C-terminally fused with mDsRed, we used the expressing vector pgPamyB-mdsred-aipA-TamyB, carrying the sequence of P*amyB*, *mdsred*, T*amyB*, and the *niaD* marker. The DNA sequence of *Aoabp1* ORF, *mdsred*, and the other plasmid were amplified by PCR using PrimeSTAR MAX DNA

polymerase and the primer sets KK320 and KK321, and KK322 and KK323, and KK318 and KK319, respectively, and ligated with the PCR-amplified sequences by In-Fusion reaction, resulting in pgPamyB-Aoabp1-mdsred-TamyB. This plasmid was introduced into strains DABP1 and DAIPADABP1 by *A. oryzae* transformation.

To construct strains expressing AoSnc1 N-terminally fused with EGFP, we used the expression vector pgPpgkA-egfp-Aosnc1-TamyB carrying the sequence of *egfp*, *Aosnc1* ORF, T*amyB* and the *niaD* marker. This plasmid was introduced into strains NSRku70-1-1AS, DAIPAS1, DABP1, and DAIPAABP1 by *A. oryzae* transformation.

Fluorescence microscopy

To observe AoCan1-EGFP, Lifeact-EGFP, EGFP-AipA, AoAbp1-mDsRed, and EGFP-AoSnc1, approximately 10^5 conidia were inoculated into 100 µl of CD or CDm-mal medium placed into poly-lysine coated glass bottom dishes (Matsunami) at 30°C for 20 h. Hyphae were observed by using a TCS SP8 inverted microscope (Leica) equipped with a 100× objective lens (1.40 numerical aperture), a HyD2 detector, an FOV scanner, and 488 nm and 561 nm argon lasers for EGFP and mDsRed fluorescence, respectively. Image data were acquired by using LAS X software (Leica). To analyze the fluorescence intensity of Lifeact-EGFP, line-scan was conducted by

208 using the NIS Elements AR software (Nikon).

209 To determine the rate of endocytosis, number of hyphae was counted at each time
210 point with intervals of 10 min. After culturing for 20 h in CD or CDm medium, cells were
211 washed once with CD+arg or CDm+arg, then shifted and observed for up to 90 min.
212 Subsequently, at every 10 min, it was determined whether there was AoCan1-EGFP
213 fluorescence remained on the plasma membrane for approximately 50 hyphal cells. An
214 inhibitor treatment using nocodazole (NOC; Sigma) was carried out as described
215 previously (Higuchi *et al*., 2006). NOC was used at a final concentration of 100 μg/mL
216 from a stock solution of 10 mg/mL suspended in DMSO.

217

218 *Expression and purification of recombinant AipA*

219 The full-length sequence of *aipA* ORF excluding intron was divided into 3 fragments
220 and amplified by PCR using KOD FX Neo DNA polymerase and the primer sets RH141
221 and RH142, and RH143 and RH144, and RH145 and RH146, respectively. pET50b(+)
222 vector (Novagen) was amplified by inverse PCR using KOD FX Neo DNA polymerase
223 and the primer sets pET50b inf Fw and pET50b inf Rv, and ligated with the PCR-
224 amplified sequences by In-Fusion reaction, resulting in pET50b(+)-aipA. The mutant
225 $AipA^{K542A}$ and $AipA^{E596Q}$ expressing vector was amplified by PCR using PrimeSTAR

Max DNA polymerase (Takara) and the primer sets RH150 and RH151, and RH152 and RH153, respectively, and ligated with the PCR-amplified sequences by In-Fusion reaction, resulting in pET50b(+)-aipA^{K542A} and pET50b(+)-aipA^{E596Q}.

Rosetta^{TM} 2(DE3) cells (Novagen) were transformed with the expression plasmids for AipA, AipA^{K542A} and AipA^{E596Q}. Cells were grown in LB media supplemented with 0.003% kanamycin and chloramphenicol at 37℃ to OD_{600}=0.5-0.8. Protein expression was induced at 48 h, 15°C with 0.5 mM isopropyl β-D-thiogalactopyranoside (IPTG). Cells were harvested by centrifugation at 8,000×g for 10 min and resuspended in lysis buffer 1 (60 mM HEPES, pH 7.6, 200 mM NaCl, 0.5 mM EDTA, 10% glycerol). The lysis buffer for AipA (lysis buffer 2) additionally contained 10 mM $MgCl_2$. Lysis buffers were supplemented with protease inhibitor.

All purification steps were performed at 4°C. Cells were lysed by sonication. The lysates were clarified by centrifugation at 15,000 rpm for 10 min and the soluble extracts were bound to HisTrap^{TM} FF 1 mL column (GE Healthcare) and washed with buffer 3 (100 mM MOPS-NaOH, pH 7.4, 500 mM NaCl, 40 mM imidazole, 1 mM ATP). The bound AipA was eluted with buffer 4 (100 mM MOPS-NaOH, pH 7.4, 500 mM NaCl, 250 mM imidazole, 1 mM ATP). The eluate was treated with HRV 3C protease (Novagen) overnight at 4°C, and was buffer exchanged using spin concentrators into

buffer 5 (60 mM HEPES, pH 7.6, 200 mM NaCl, 10 mM $MgCl_2$, 1 mM ATP). Protein solutions were then passed over fresh His-Trap to remove the HRV 3C protease and uncleaved protein. The flow-through was collected and concentrated using Amicon Ultra spin concentrator (Millipore) with appropriate molecular weight cut-offs. Then the concentrated protein was buffer exchanged using spin concentrators into buffer 6 (60 mM HEPES, pH7.6, 200 mM NaCl, 10 mM $MgCl_2$, 1 mM ATP, 5% glycerol). Protein concentration was measured using the BCA Protein Assay Kit (Takara).

ATPase assay

ATP hydrolysis rates were determined using a spectrophotometric assay that couples ADP formation to the depletion of NADH (Nørby 1988; Olszewski *et al*. 2019). AipA and ATPase mix were incubated separately at 30°C for 20 min and then combined in 96-well plate (Greiner). Absorbance at 340 nm was monitored in 15 sec intervals for 25 min with a flexible microplate reader InfiniteF200PRO (Tecan). Reaction was performed in 1×ATPase mix (5 mM ATP, 3 U mL^{-1} pyruvate kinase (Sigma), 3 U mL^{-1} lactate dehydrogenase (Sigma), 1 mM NADH, 7.5 mM phosphoenol pyruvate (Sigma)) and buffer 7 (60 mM HEPES, pH7.6, 200 mM NaCl, 10 mM $MgCl_2$, 5% glycerol). ATPase rate was extracted from the linear region of the absorbance trace using the

262 extinction coefficient for NADH (6.22 mM^{-1} cm^{-1}).

263

264 *Quantitative RT-PCR analysis*

265 Quantitative reverse transcription PCR (qRT-PCR) analysis was performed as
266 described previously (Togo et al. 2017). Total RNA was extracted from cells of each
267 strain cultured in 200 mL of CD or CDm-mal medium for 2 days, and cDNA was
268 synthesized using a SuperPrep Cell Lysis & RT Kit for qPCR (TOYOBO). qRT-PCR
269 analysis of each cDNA sample was carried out in triplicate by using a Thermal Cycler
270 Dice Real Time System TP-800 instrument (Takara) and Thunderbird SYBR qPCR Mix
271 (TOYOBO). The mRNA expression level of *aipA* was determined by using the primer
272 set YHK255 and YHK256. The expression of the gene was normalized to that of *gpdA*
273 (AO090003001322) determined by the primers YHK196 and YHK197.

274

Results

Endocytosis of AoCan1 is facilitated in ΔaipA and delayed in ΔAoabp1 cells

To investigate how AipA and AoAbp1 are involved in endocytosis in *A. oryzae*, we analyzed endocytosis of the arginine permease AoCan1 tagged with EGFP in the Δ*aipA* or Δ*Aoabp1* background, using the way reported before (Matsuo *et al.* 2013). Generally, since the amount of transporters localized at the apical plasma membrane is less than other hyphal regions, we investigated endocytosis of AoCan1-EGFP at around hyphal middle regions (Hayakawa *et al*. 2011). AoCan1-EGFP was gradually taken up from the plasma membrane into cells by endocytosis when the observation medium was changed to one containing arginine, and the EGFP fluorescence on the plasma membrane disappeared. To monitor the endocytic process in detail, approximately 50 cells were observed every 10 min for a total of 90 min, and the presence or absence of AoCan1-EGFP fluorescence at the plasma membrane was counted as endocytosis occurred or not. In control and Δ*aipA* strains, AoCan1-EGFP at the plasma membrane was lost at 90 min after the medium shift (Fig. 1A, B). However, at 50 and 70 min points, endocytosis of AoCan1-EGFP was facilitated in the Δ*aipA* strain compared with the control strain (Fig. 1B). Next, we investigated the Δ*Aoabp1* cells for endocytosis and found that the fluorescence of AoCan1-EGFP remained at the

293 plasma membrane even at 90 min after the induction of endocytosis (Fig. 2A, B). In
294 contrast, in the complement *Aoabp1* strain, the fluorescence of AoCan1-EGFP was
295 disappeared almost as much as the control strain (Fig. 2A, B). These results suggested
296 that AipA and AoAbp1 are negative and positive regulators of AoCan1 endocytosis,
297 respectively, in *A. oryzae*.
298 Actin cytoskeleton is closely related to endocytosis in filamentous fungi (Upadhyay
299 & Shaw 2008; Higuchi *et al*. 2009a; Echauri-Espinosa *et al*. 2012). To visualize
300 filamentous actin (F-actin) dynamics, we used actin marker protein Lifeact fused with
301 EGFP (Riedl J *et al*. 2008; Hayakawa *et al*. 2011; Mamun *et al.* 2020), and found that
302 the localization of F-actin was concentrated at the tip of the hypha in Δ*aipA* strain; in
303 contrast, in Δ*Aoabp1* and Δ*aipA*Δ*Aoabp1* strains, it was similar to control strain (Fig.
304 3A, B). Therefore, it was suggested that AipA may negatively regulate the
305 polymerization of F-actin via AoAbp1, and that there are other proteins which have
306 similar function to AoAbp1.
307 Endocytosis in filamentous fungi can be broadly divided into two types by cargo,
308 destination, and proteins involved in the process. The first is the case where it goes to
309 the vacuole after endocytosis for degradation, and it is considered that transporters,
310 such as AoUapC and AoCan1, are endocytosed in which clathrin is involved. The

311 second is the case of recycling to the tip of the hyphae after endocytosis. Membrane
312 proteins that are mainly localized in the endocytic collar, such as SNARE proteins and
313 flippase, are the cargoes of endocytosis, and the AP-2 complex is thought to play an
314 important role (Marzoukou *et al*. 2017). Based on such information, we investigated the
315 function of AipA and AoAbp1 by analyzing the localization of EGFP-AoSnc1, which is
316 considered to be the cargo of the latter apical endocytic recycling. It was reported that
317 in the endocytosis-defective strain, AoSnc1 loses its apical polarity and is uniformly
318 localized at the plasma membrane (Higuchi *et al*. 2009a). However, the localization of
319 EGFP-AoSnc1 in Δ*aipA* and Δ*Aoabp1* strains was not different from that of the control
320 strain (Fig. S1). In addition, the phenotypic change on growth was not observed in the
321 Δ*aipA* and Δ*Aoabp1* strains (Fig. S2). Collectively, it was suggested that neither AipA
322 nor AoAbp1 has crucial roles in apical endocytic recycling of AoSnc1 and cell viability.
323
324 *AipA localization is dependent on the presence of AoAbp1*
325 In our previous study, AipA was identified as a protein interacted with AoAbp1
326 (Higuchi *et al.* 2011). Indeed, AipA colocalizes with AoAbp1 at the endocytic sites of
327 apical regions. To examine which protein functions upstream in endocytosis, we
328 observed the localization of these proteins in each mutant strain. In the Δ*aipA* strain,

AoAbp1-mDsRed localized at the tip of hyphae as in the control strain (Fig. 4A), indicating that the localization of AoAbp1 is independent of AipA. However, in the Δ*Aoabp1* strain, EGFP-AipA was dispersed and localized at dots in the hyphal cytoplasm (Fig. 4A), suggesting that the localization of AipA at the endocytic sites depends on the presence of AoAbp1.

Previously, we demonstrated that the interaction between AipA and AoAbp1 occurs in the proline-rich region (346-370 aa) of AipA and the SH3 domains of AoAbp1. Therefore, we investigated whether interaction with AoAbp1 is important for the localization of AipA, and found that EGFP-AipA$^{\Delta 346\text{-}370}$ was dispersed in the cytoplasm (Fig. 4B). This result revealed that the localization of AipA at the endocytic sites depends on the interaction between AipA and AoAbp1. Moreover, we examined whether AAA ATPase activity is important for the localization of AipA. In our previous study, we determined that the AAA ATPase domain of AipA is highly conserved with that of *S. cerevisiae* AAA ATPases Sap1p, Yta6p, and Vps4p (Babst *et al.* 1997, 1998; Higuchi *et al.* 2011). Therefore, for the analysis of the AAA ATPase domain of AipA, two point mutations AipA^{K542A} and AipA^{E596Q} were introduced. K542A of AipA is a mutation to Walker A, which is an ATP binding site, and E596Q of AipA is a mutation to Walker B, which is an ATP hydrolytic active site. By using recombinant proteins, we determined

347 that the ATPase activity of AipA^{K542A} and AipA^{E596Q} were 23% and 28%, respectively,
348 lower than that of the wild-type AipA (Fig. S3). Next, we generated strains expressing
349 EGFP-AipA^{K542A} or EGFP-AipA^{E596Q} and found that EGFP-AipA^{K542A} localized at the tip
350 of hyphae as in the control strain; on the other hand, EGFP-AipA^{E596Q} localized at both
351 the tip and basal regions of hyphae (Fig. 4C). These results suggested that the K542A
352 mutation of AipA does not affect the localization of AipA, but the E596Q mutation
353 seems to be more important for its localization than the K542A mutant.
354
355 *Endocytosis of AoCan1-EGFP is delayed in ΔaipAΔAoabp1 cells*
356 To further study about the functional dependency of AipA and AoAbp1, we analyzed
357 endocytosis of AoCan1-EGFP in the Δ*aipA*Δ*Aoabp1* strain. The fluorescence of
358 AoCan1-EGFP remained at the plasma membrane even at 90 min after the induction of
359 endocytosis in Δ*aipA*Δ*Aoabp1* cells, and the cells that endocytosis of AoCan1-EGFP
360 occurred were only 27% compared with the control cells (Fig. 5A, B). These results
361 were similar to that of AoCan1 endocytosis in Δ*Aoabp1* strain, suggesting that the
362 deletion effect of *Aoabp1* was more significant than that of *aipA* in endocytosis of
363 AoCan1-EGFP. Moreover, we found that the localization of Lifeact-EGFP (Fig. 3),

364 EGFP-AoSnc1 (Fig. S1) and the growth phenotype (Fig. S2) were not changed in the
365 Δ*aipA*Δ*Aoabp1* strain compared with the control strain.
366
367 *Analysis of AoCan1-EGFP endocytosis in the aipA-overexpressing strains*
368 To investigate an effect of *aipA*-overexpression, we analyzed endocytosis of
369 AoCan1-EGFP in the *aipA*-overexpressing strain. We confirmed that the mRNA
370 expression level of the strain was more than 10-fold higher than that of the control
371 strain (Fig. S4). Endocytosis of AoCan1-EGFP was delayed especially at 30 min and
372 later after the medium shift in the *aipA*-overexpressing strain compared with the control
373 strain (Fig. 6A, B). Then, to investigate effects of the AipA^{K542A} and AipA^{E596Q} mutations,
374 we also monitored endocytosis of AoCan1-EGFP in *aipA*^{K542A}- and *aipA*^{E596Q}-
375 overexpressing strains, and the mRNA expression levels of these strains were about
376 10-fold higher than that of the control strain (Fig. S4). We found that endocytosis of
377 AoCan1-EGFP in the *aipA*^{K542A}-overexpressing strain was almost same with that in the
378 control background and faster than that in the *aipA*-overexpressing strain at 30, 80 and
379 90 min after the medium shift (Fig. 6A, B). It was also found that, in the *aipA*^{E596Q}-
380 overexpressing strain, endocytosis of AoCan1-EGFP was facilitated at 30, 50, 70 and
381 80 min, compared with the *aipA*-overexpressing strain (Fig. 6A, B). These results

suggested that the negative effect of *aipA*-overexpression in endocytosis was dependent on the function of AAA ATPase activity of AipA. Moreover, we found that overexpressed EGFP-AipA, EGFP-AipA^{K542A} and EGFP-AipA^{E596Q} were localized along microtubule, which was confirmed by a treatment using a microtubule depolymerizing reagent nocodazole (Fig. 7). Furthermore, EGFP-AipA^{K542A} and EGFP-AipA^{E596Q} were accumulated at the hyphal tip more than EGFP-AipA, suggesting that this localization change might reduce the negative function in endocytosis of AoCan1 (Fig. 7). The localization patterns of EGFP-AipA^{K542A} and EGFP-AipA^{E596Q} in Fig. 7 were different from those in Fig. 4C. This was likely because of the different strain backgrounds: in Fig. 4C, native *aipA* was deleted and EGFP-fused proteins were moderately expressed, while in Fig. 7, native *aipA* existed and EGFP-fused proteins were overexpressed.

Analysis of AoCan1-EGFP endocytosis in the aipA-complementary strains

Finally, we analyzed endocytosis of AoCan1-EGFP in *aipA*-complementary strain, in which *aipA* was introduced under the control of the native promoter into the *aipA* disruptant strain. We confirmed that the mRNA expression levels were almost the same among the generated strains (Fig. S5). At 10, 20 and 40 min points after the medium

400 shift, the population of cells with endocytosis of AoCan1-EGFP in the *aipA*-
401 complementary strain was lower than that in the Δ*aipA* strain, and there was a
402 tendency that the function of AipA was complemented, although there was no
403 significant difference (Fig. 8A, B). On the other hand, unexpectedly, in the *aipA*^{K542A}-
404 expressing strain in the *aipA* deletion background, endocytosis of AoCan1-EGFP was
405 faster than other three strains and there was a significant difference at 50 min after the
406 medium shift (Fig. 8A, B). Moreover, in the *aipA*^{E596Q}-expressing strain in the *aipA*
407 deletion background, endocytosis of AoCan1-EGFP was facilitated at 20-90 min
408 compared to the Δ*aipA* strain, although there was no significant difference (Fig. 8A, B).
409 These results suggested that AipA^{K542A} and AipA^{E596Q} may behave differently with or
410 without wild-type AipA, and that mutations K542A and E596Q in the AAA ATPase
411 domain have different effects on AipA function.

412 **Discussion**

413 In this study, we revealed the function of AipA to negatively control endocytosis of
414 the arginine permease AoCan1 fused with EGFP in *A. oryzae*. Although endocytosis of
415 AoCan1-EGFP was delayed in the Δ*Aoabp1* and Δ*aipA*Δ*Aoabp1* strains, it was
416 accelerated in the Δ*aipA* strains compared to the control strains. Moreover, in the *aipA*-
417 overexpressing strain, the uptake of AoCan1-EGFP was decreased, whereas in the
418 mutant *aipA*-overexpressing strain in which AAA ATPase activity was reduced, this
419 endocytic defect was not observed. Collectively, our data further clarified that AipA
420 negatively regulates endocytosis of AoCan1.

421 We also revealed that AoAbp1, as an AipA-interacting protein, was involved in
422 endocytosis of AoCan1-EGFP, although Δ*Aoabp1* cells did not exhibit any significant
423 growth defect. In the rice blast fungus *Magnaporthe oryzae*, the growth of Δ*Moabp1*
424 cells is very severely inhibited and the internalization of FM4-64 was delayed in the
425 hyphae of the Δ*Moabp1* mutant. The internalization of FM4-64 did not occur until 4 min
426 after the staining in about 76% of the mutant hyphae, while it occurred after 1 min in
427 the wild-type strain (Li *et al.* 2019). In *S. cerevisiae*, *abp1*Δ showed no significant
428 difference from wild-type cells in the behavior of generally used endocytic factors and
429 in the uptake nor subsequent trafficking of FM4-64 (Kaksonen *et al.* 2005;

Aghamohammadzadeh *et al.* 2014). However, *abp1* deletion is lethal when combined with other gene deletion, *sla1*Δ, *sla2*Δ, and *sac6*Δ, suggesting that Abp1 seems to be multifunctional, and the functional activity of Abp1 might be overlapped with that of Sla1, Sla2, and Sac6 (Pollard & Cooper 1986; Hartwig & Kwiatkowski 1991; Holtzman *et al*. 1993). Therefore, it was suggested that there might be some protein(s) which has a complementary function with AoAbp1 for the growth of *A. oryzae.* Furthermore, our localization analysis using the Δ*aipA* and Δ*Aoabp1* strains suggested that AipA functions downstream of AoAbp1 in AoCan1 endocytosis.

According to the estimated amino-acid sequence of AipA, AAA ATPase domain is located at the C-terminal region. The ATPase domain of AAA+ proteins forms oligomers that are predominantly hexametric and are always ring-shaped with a central cavity (White & Lauring 2007; Puchades *et al.* 2020). ATP binding and hydrolysis are obviously required to provide the energy for AAA+ proteins to remodel their substrate proteins. AipA is predicted to be a type I AAA+ protein from the amino acid sequence. The same type I AAA ATPase as AipA includes katanin and spastin that have been studied in advance in mammalian cells, and these proteins use the ATPase activity for disassembly of tubulin polymers (Puchades *et al*. 2020). The N-terminal region of katanin and spastin, a microtubule-interacting and -trafficking (MIT) domain, recognizes

448 microtubules (Roll-Mecak & Vale 2008; Roll-Mecak & McNally 2010). In contrast, AipA
449 does not have a domain homologous to the MIT domain, but EGFP-AipA seemed to be
450 localized at microtubules in the *aipA*-overexpressing background. Therefore, although
451 AipA does not have the MIT domain, it is suggested that AipA has a spastin-like
452 function with affinity to microtubules. On the other hand, in the hyphal tip of Δ*aipA* cells,
453 actin cytoskeleton was more accumulated compared with the control cells, suggesting
454 that AipA might have a function of negatively regulating the F-actin polymerization via
455 AoAbp1. It was also suggested that there are some other proteins which have a
456 function similar to AoAbp1.
457 Although recombinant AipA^{K542A} and AipA^{E596Q} still retained more than 70% residual
458 ATPase activity, there was significant difference in endocytosis of AoCan1-EGFP
459 between the *aipA*-overexpressing strain and *aipA*^{K542A}- or *aipA*^{E596Q}-overexpressing
460 strains. In *Drosophila melanogaster*, the mutant E561A of Spastin, which is important
461 for substrate binding to its substrate, microtubules, causes difficulty in capturing
462 microtubules, so that mutation of E561 abolishes severing while still retaining about
463 75% ATPase activity of wild-type Spastin (Sandate *et al*. 2019). Although the substrate
464 for AipA has not yet been discovered, it is possible that it may become a functional
465 deletion even if the ATPase activity was not decreased dramatically like Spastin in *D*.

466 *melanogaster*.

467 We found phenotypic differences of AipA^{K542A} and AipA^{E596Q} in endocytosis of
468 AoCan1-EGFP between the strain backgrounds of overexpression and
469 complementation (Fig. 9). AipA^{K542A} promoted endocytosis of AoCan1-EGFP, but its
470 overexpression in the presence of AipA did not. In contrast, overexpression of AipA^{E596Q}
471 in the presence of AipA enhanced endocytosis of AoCan1-EGFP, but AipA^{E596Q} itself did
472 not. Since it was previously shown that AipA interacts with itself (Higuchi *et al*. 2011),
473 these phenotypic differences might be caused by interaction between AipA and its
474 mutant. In addition, we found that the localization patterns of AipA^{K542A} and AipA^{E596Q}
475 were different, which might cause difference in endocytosis. It was also suggested that
476 AipA might use different functions depending on the ATPase activity, and it can be
477 considered that the mutations in AAA ATPase domain enable AipA to participate in
478 different mechanisms in endocytosis of AoCan1. In the future, it is necessary to
479 proceed with a more detailed analysis of the molecular function of AipA in endocytosis
480 by discovering an unknown AipA substrate, except for AoAbp1, and investigating the
481 relationship between ATPase activity and the substrate.

482

483

Acknowledgments

We would like to thank the Center for Advanced Instrumental and Educated Supports at Faculty of Agriculture, Kyushu University for technical help with fluorescence microscopy. We also would like to thank Drs. Yoshinori Katakura and Kiichiro Teruya for technical supports in qRT-PCR analysis and ATPase assay, respectively. This study was supported in part by JSPS KAKENHI [Grant No. JP19H02874 (Y.H.)] and the Sasakawa Scientific Research Grant from The Japan Science Society (R.H.).

References

Aghamohammadzadeh S, Smaczynska-de Rooij II, Ayscough KR, 2014. An Abp1-dependent route of endocytosis functions when the classical endocytic pathway in yeast is inhibited. *PLOS ONE* **9**: e103311.

Araujo-Bazán L, Peñalva MA, Espeso EA, 2008. Preferential localization of the endocytic internalization machinery to hyphal tips underlies polarization of the actin cytoskeleton in *Aspergillus nidulans*. *Molecular Microbiology* **67** :891-905.

Babst M, Sato TK, Banta LM, Emr SD, 1997. Endosomal transport function in yeast requires a novel AAA-type ATPase, Vps4p. *EMBO Journal* **16** :1820-31.

502 Babst M, Wendland B, Estepa EJ, Emr SD, 1998. The Vps4p AAA ATPase regulates
503 membrane association of a Vps protein complex required for normal endosome
504 function. *EMBO Journal* **17** : 2982-93.
505 Bartnicki-Garcia S, Garduño-Rosales M, Delgado-Alvarez DL, Mouriño-Pérez RR,
506 2018. Experimental measurement of endocytosis in fungal hyphae. *Fungal Genetics*
507 *and Biology* **118** :32-36.
508 Echauri-Espinosa RO, Callejas-Negrete OA, Roberson RW, Bartnicki-García S,
509 Mouriño-Pérez RR, 2012. Coronin is a component of the endocytic collar of hyphae
510 of *Neurospora crassa* and is necessary for normal growth and morphogenesis.
511 *PLOS ONE* **7** :e38237.
512 Grossmann G, Malinsky J, Stahlschmidt W, Loibl M, Weig-Meckl I, Frommer WB,
513 Opekarová M, Tanner W, 2008. Plasma membrane microdomains regulate turnover
514 of transport proteins in yeast. *Journal of Cell Biology* **183** :1075-88.
515 Hartwig JH, Kwiatkowski DJ 1991. Actin-binding proteins. *Current Opinion in Cell*
516 *Biology* **3** :87-97.
517 Hayakawa Y, Ishikawa E, Shoji JY, Nakano H, Kitamoto K, 2011. Septum-directed
518 secretion in the filamentous fungus *Aspergillus oryzae*. *Molecular Microbiology*
519 **81** :40-55.

520 Higuchi Y, Nakahama T, Shoji JY, Arioka M, Kitamoto K, 2006. Visualization of the
521 endocytic pathway in the filamentous fungus *Aspergillus oryzae* using an EGFP-
522 fused plasma membrane protein. *Biochemical and Biophysical Research*
523 *Communications* **340** :784-91.
524 Higuchi Y, Shoji JY, Arioka M, Kitamoto K, 2009a. Endocytosis is crucial for cell polarity
525 and apical membrane recycling in the filamentous fungus *Aspergillus oryzae*.
526 *Eukaryotic Cell* **8** :37-46.
527 Higuchi Y, Arioka M, Kitamoto K, 2009b. Endocytic recycling at the tip region in the
528 filamentous fungus *Aspergillus oryzae*. *Communicative and Integrative Biology*
529 **2** :327-8.
530 Higuchi Y, Arioka M, Kitamoto K, 2011. Functional analysis of the putative AAA
531 ATPase AipA localizing at the endocytic sites in the filamentous fungus *Aspergillus*
532 *oryzae*. *FEMS Microbiology Letters* **320** :63-71.
533 Higuchi Y, 2021a. Membrane traffic related to endosome dynamics and protein
534 secretion in filamentous fungi. *Bioscience, Biotechnology, and Biochemistry*
535 **85** :1038-1045.
536 Higuchi Y, 2021b. Membrane traffic in *Aspergillus oryzae* and related filamentous fungi.
537 *Journal of Fungi* **7** :534.

538 Hiramoto T, Tanaka M, Ichikawa T, Matsuura Y, Hasegawa-Shiro S, Shintani T, Gomi
539 K, 2015. Endocytosis of a maltose permease is induced when amylolytic enzyme
540 production is repressed in *Aspergillus oryzae*. *Fungal Genetics and Biology*
541 **82** :136-44.
542 Holtzman DA, Yang S, Drubin DG, 1993. Synthetic-lethal interactions identify two novel
543 genes, SLA1 and SLA2, that control membrane cytoskeleton assembly in
544 *Saccharomyces cerevisiae*. *Journal of Cell Biology* **122** :635-44.
545 Kaksonen M, Toret CP, Drubin DG, 2005. A modular design for the clathrin- and actin-
546 mediated endocytosis machinery. *Cell* **123** :305-20.
547 Kim K, Galletta BJ, Schmidt KO, Chang FS, Blumer KJ, Cooper JA, 2006. Actin-based
548 motility during endocytosis in budding yeast. *Molecular Biology of the Cell* **17** :1354-
549 63.
550 Lara-Rojas F, Bartnicki-García S, Mouriño-Pérez RR, 2016. Localization and role of
551 MYO-1, an endocytic protein in hyphae of *Neurospora crassa*. *Fungal Genetics and*
552 *Biology* **88**: 24-34.
553 Li L, Zhang S, Liu X, Yu R, Li X, Liu M, Zhang H, Zheng X, Wang P, Zhang Z, 2019.
554 *Magnaporthe oryzae* Abp1, a MoArk1 Kinase-Interacting Actin Binding Protein,
555 Links Actin Cytoskeleton Regulation to Growth, Endocytosis, and Pathogenesis.

Molecular Plant-Microbe Interactions Journal **32** :437-451.

Mamun MAA, Katayama T, Cao W, Nakamura S, Maruyama JI, 2020. A novel Pezizomycotina-specific protein with gelsolin domains regulates contractile actin ring assembly and constriction in perforated septum formation. *Molecular Microbiology* **113** :964-982.

Martzoukou O, Amillis S, Zervakou A, Christoforidis S, Diallinas G, 2017. The AP-2 complex has a specialized clathrin-independent role in apical endocytosis and polar growth in fungi. *eLife* **6** :e20083.

Matsuo K, Higuchi Y, Kikuma T, Arioka M, Kitamoto K, 2013. Functional analysis of Abp1p-interacting proteins involved in endocytosis of the MCC component in *Aspergillus oryzae*. *Fungal Genetics and Biology* **56** :125-34.

McDermott H, Kim K, 2015. Molecular dynamics at the endocytic portal and regulations of endocytic and recycling traffics. *European Journal of Cell Biology* **94** :235-48.

Nørby JG, 1988. Coupled assay of Na+,K+-ATPase activity. *Methods in Enzymology* **156** :116-9.

Olszewski MM, Williams C, Dong KC, Martin A, 2019. The Cdc48 unfoldase prepares well-folded protein substrates for degradation by the 26S proteasome. *Communications Biology* **2** :29.

574 Pantazopoulou A, Peñalva MA, 2011. Characterization of *Aspergillus nidulans*
575 RabC/Rab6. *Traffic* **12** :386-406.
576 Peñalva MA, 2005. Tracing the endocytic pathway of *Aspergillus nidulans* with FM4-64.
577 *Fungal Genetics and Biology* **42** :963-75.
578 Peñalva MA, 2010. Endocytosis in filamentous fungi: Cinderella gets her reward.
579 *Current Opinion in Microbiology* **13** :684-692.
580 Pollard TD, Cooper JA 1986. Actin and actin-binding proteins. A critical evaluation of
581 mechanisms and functions. *Annual Review of Biochemistry* **55** :987-1035.
582 Polo S, Di Fiore PP, 2006. Endocytosis conducts the cell signaling orchestra. *Cell*
583 **124** :897-900.
584 Puchades C, Sandate CR, Lander GC , 2020. The molecular principles governing the
585 activity and functional diversity of AAA+ proteins. *Nature Reviews Molecular Cell*
586 *Biology* **21** :43-58.
587 Riedl J, Crevenna AH, Kessenbrock K, Yu JH, Neukirchen D, Bista M, Bradke F, Jenne
588 D, Holak TA, Werb Z, Sixt M, Wedlich-Soldner R, 2008. Lifeact: a versatile marker
589 to visualize F-actin. *Nature Methods* **5** :605-7.
590 Roll-Mecak A, McNally FJ, 2010. Microtubule-severing enzymes. *Current Opinion in*
591 *Cell Biology* **22** :96-103.

592 Roll-Mecak A, Vale RD, 2008. Structural basis of microtubule severing by the
593 hereditary spastic paraplegia protein spastin. *Nature* **451** :363-7.
594 Sandate CR, Szyk A, Zehr EA, Lander GC, Roll-Mecak A, 2019. An allosteric network
595 in spastin couples multiple activities required for microtubule severing. *Nature*
596 *Structural & Molecular Biology* **26** : 671-678.
597 Schultzhaus Z, Yan H, Shaw BD, 2015. *Aspergillus nidulans* flippase DnfA is cargo of
598 the endocytic collar and plays complementary roles in growth and
599 phosphatidylserine asymmetry with another flippase, DnfB. *Molecular Microbiology*
600 **97** :18-32.
601 Shaw BD, Chung DW, Wang CL, Quintanilla LA, Upadhyay S, 2011. A role for
602 endocytic recycling in hyphal growth. *Fungal Biology* **115** :541-6.
603 Shoji JY, Kikuma T, Kitamoto K, 2014. Vesicle trafficking, organelle functions, and
604 unconventional secretion in fungal physiology and pathogenicity. *Current Opinion in*
605 *Microbiology* **20** :1-9.
606 Taheri-Talesh N, Horio T, Araujo-Bazán L, Dou X, Espeso EA, Peñalva MA, Osmani
607 SA, Oakley BR, 2008. The tip growth apparatus of *Aspergillus nidulans*. *Molecular*
608 *Biology of the Cell* **19** :1439-49.
609 Togo Y, Higuchi Y, Katakura Y, Takegawa K, 2017. Early endosome motility mediates

610 α-amylase production and cell differentiation in *Aspergillus oryzae*. *Scientific*
611 *Reports* **7** :15757.
612 Upadhyay S, Shaw BD, 2008. The role of actin, fimbrin and endocytosis in growth of
613 hyphae in *Aspergillus nidulans*. *Molecular Microbiology* **68** :690-705.
614 White SR, Lauring B, 2007. AAA+ ATPases: achieving diversity of function with
615 conserved machinery. *Traffic* **8** :1657-67.

616 **Table 1 *A. oryzae* strains used in this study.**

Strain	Genotype	Reference
RIB40	Wild-type	
NSRku70-1-1A	*niaD- sC- adeA- adeA ΔargB Δku70::argB*	Higuchi et al. (2009a)
NSRku70-1-1AN	*niaD–::niaD sC– adeA– adeA ΔargB Δku70::argB*	Higuchi et al.(2011)
DAIPA1-com	*niaD–::(PaipA-aipA-TaipA niaD) sC– adeA– ΔaipA::adeA ΔargB Δku70::argB*	Higuchi et al.(2011)
PaaA1	*niaD–::(PamyB-aipA niaD) sC– adeA–::adeA ΔargB Δku70::argB*	Higuchi et al.(2011)
PaaA5421	*niaD–::(PamyB-aipA^{K542A} niaD) sC– adeA–::adeA ΔargB Δku70::argB*	Higuchi et al.(2011)
PaaA5961	*niaD-::(PamyB-aipA^{E596Q} niaD) sC- adeA-::adeA ΔargB Δku70::argB*	Higuchi et al.(2011)
PaEaASO1	*niaD– niaD sC–::(PamyB-egfp-aipA AosC) adeA–::adeA ΔargB Δku70::argB*	Higuchi et al.(2011)

PaEaA542SO1	*niaD-::niaD sC-::(PamyB-egfp-aipAK542A AosC) adeA-::adeA ΔargB Δku70::argB*	Higuchi et al.(2011)
PaEaA596SO1	*niaD-::niaD sC-::(PamyB-egfp-aipAE596Q AosC) adeA-::adeA ΔargB Δku70::argB*	Higuchi et al.(2011)
DAIPA1	*niaD- sC- adeA- ΔaipA::adeA ΔargB Δku70::argB*	Higuchi et al.(2011)
NSRku70-1-1ANSO	*niaD-::niaD sC-::AosC adeA-::adeA ΔargB Δku70::argB*	This study
DAIPA1-N	*niaD-::niaD sC- adeA- ΔaipA::adeA ΔargB Δku70::argB*	This study
DAIPA1-NS	*niaD-::niaD sC-::AosC adeA- ΔaipA::adeA ΔargB Δku70::argB*	This study
DAIPAS1-PaEA	*niaD– ::(PamyB-egfp-aipA niaD) sC–::AosC adeA- ΔaipA::adeA ΔargB Δku70::argB*	This study
DABP1-PaAD	*niaD– ::(PamyB-Aoabp1-mdsred niaD) sC– ΔAoabp1::AosC adeA–::adeA ΔargB Δku70::argB*	This study

DAIPAABP1-PaEA	*niaD– ::(PamyB-egfp-aipA niaD) sC– ΔAoabp1::AosC adeA– ΔaipA::adeA ΔargB Δku70::argB*	This study
DAIPAABP1-PaAD	*niaD– ::(PamyB-Aoabp1-mdsred niaD) sC– ΔAoabp1::AosC adeA– ΔaipA::adeA ΔargB Δku70::argB*	This study
NSRku70-1-1AS	*niaD– sC–::AosC adeA–::adeA ΔargB Δku70::argB*	This study
DAIPAS1	*niaD– sC–::AosC adeA– ΔaipA::adeA ΔargB Δku70::argB*	This study
DAIPAS1-PaEA542	*niaD–::(PamyB-egfp-aipA^{K542A} niaD) sC–::AosC adeA– ΔaipA::adeA ΔargB Δku70::argB*	This study
DAIPAS1-PaEA596	*niaD–::(PamyB-egfp-aipA^{E596Q} niaD) sC–::AosC adeA– ΔaipA::adeA ΔargB Δku70::argB*	This study
DAIPAS1-PaEA346-370	*niaD–::(PamyB-egfp-aipAΔ346-370 niaD) sC–::AosC adeA– ΔaipA::adeA ΔargB Δku70::argB*	This study
DABP1	*niaD– sC– ΔAoabp1::AosC adeA– adeA ΔargB Δku70::argB*	This study

DAIPAABP1	*niaD– sC– ΔAoabp1::AosC adeA– ΔaipA::adeA ΔargB Δku70::argB*	This study
Can1E	*niaD–::niaD sC–::AosC adeA–::adeA ΔargB Δku70::argB ptrA::(Aocan1-egfp ptrA)*	This study
DAIPA1-Can1E	*niaD–::niaD sC–::AosC adeA– ΔaipA::adeA ΔargB Δku70::argB ptrA::(Aocan1-egfp ptrA)*	This study
DAIPA1-N-Can1E	*niaD-::niaD sC- adeA- ΔaipA::adeA ΔargB Δku70::argB ptrA::(Aocan1-egfp ptrA)*	This study
DAIPA1-N-Can1E-p	*niaD-::niaD sC-::AosC adeA- ΔaipA::adeA ΔargB Δku70::argB ptrA::(Aocan1-egfp ptrA)*	This study
DAIPA1-N-Can1E-com	*niaD-::niaD sC-::(PaipA-aipA-TaipA AosC) adeA- ΔaipA::adeA ΔargB Δku70::argB ptrA::(Aocan1-egfp ptrA)*	This study
DAIPA1-N-Can1E-com542	*niaD-::niaD sC-::(PaipA-aipA^{K542A}-TaipA AosC) adeA- ΔaipA::adeA ΔargB Δku70::argB ptrA::(Aocan1-egfp ptrA)*	This study

	niaD-::niaD sC-::(PaipA-aipA^{E596Q}-TaipA AosC)	
DAIPA1-N-		
	adeA- ΔaipA::adeA ΔargB Δku70::argB	This study
Can1E-com596		
	ptrA::(Aocan1-egfp ptrA)	
	niaD–::(PaipA-aipA-TaipA niaD) sC– adeA–	
DAIPA1-com-		
	ΔaipA::adeA ΔargB Δku70::argB ptrA::(Aocan1-	This study
Can1E		
	egfp ptrA)	
	niaD–::(PamyB-aipA niaD) sC– adeA–::adeA	
PaaA1-Can1E		This study
	ΔargB Δku70::argB ptrA::(Aocan1-egfp ptrA)	
PaaA5421-	*niaD–::(PamyB-aipA^{K542A} niaD) sC– adeA–::adeA*	
		This study
Can1E	*ΔargB Δku70::argB ptrA::(Aocan1-egfp ptrA)*	
PaaA5961-	*niaD-::(PamyB-aipA^{E596Q} niaD) sC- adeA-::adeA*	
		This study
Can1E	*ΔargB Δku70::argB ptrA::(Aocan1-egfp ptrA)*	
NSRku70-1-	*niaD–::(Aocan1-egfp niaD) sC–::AosC*	
		This study
1AS-Can1E	*adeA–::adeA ΔargB Δku70::argB*	
	niaD–::(Aocan1-egfp niaD) sC– ΔAoabp1::AosC	
DABP1-Can1E		This study
	adeA–::adeA ΔargB Δku70::argB	
DABP1-Can1E-	*niaD–::(Aocan1-egfp niaD) sC– ΔAoabp1::AosC*	
		This study
p	*adeA–::adeA ΔargB Δku70::argB ptrA::ptrA*	

DABP1-Can1E-com	*niaD–::(Aocan1-egfp niaD) sC– ΔAoabp1::AosC adeA–::adeA ΔargB Δku70::argB ptrA::(PAoabp1-Aoabp1-TAoabp1 ptrA)*	This study
DAIPAABP1-Can1E	*niaD–::(Aocan1-egfp niaD) sC– ΔAoabp1::AosC adeA– ΔaipA::adeA ΔargB Δku70::argB*	This study
NSRku70-1-1AS-LAE	*niaD–::(PpgkA-Lifeact-egfp niaD) sC–::AosC adeA–::adeA ΔargB Δku70::argB*	This study
DAIPAS1-LAE	*niaD–::(PagkA-Lifeact-egfp niaD) sC–::AosC adeA– ΔaipA::adeA ΔargB Δku70::argB*	This study
DABP1-LAE	*niaD–::(PpgkA-Lifeact-egfp niaD) sC– ΔAoabp1::AosC adeA– adeA ΔargB Δku70::argB*	This study
DAIPAABP1-LAE	*niaD–::(PpgkA-Lifeact-egfp niaD) sC– ΔAoabp1::AosC adeA– ΔaipA::adeA ΔargB Δku70::argB*	This study
PpES	*niaD- ::(PpgkA-egfp-Aosnc1 niaD) sC-::AosC adeA-::adeA ΔargB Δku70::argB*	This study
DAIPAS1-PpES	*niaD-::(PpgkA-egfp-Aosnc1 niaD) sC-::AosC adeA-ΔaipA::adeA ΔargB Δku70::argB*	This study

DABP1-PpES	*niaD-::(PpgkA-egfp-Aosnc1 niaD) sC-ΔAoabp1::AosC adeA-::adeA ΔargB Δku70::argB*	This study
DAIPADABP1-PpES	*niaD-::(PpgkA-egfp-Aosnc1 niaD) sC-ΔAoabp1::AosC adeA- ΔaipA::adeA ΔargB Δku70::argB*	This study

617

618 **Table 2 Primers used in this study.**

Name	Sequence (5' to 3')
KK134	GATTTAGTTCCGTTCGTGCAGG
KK217	ATGGGGTGACGATGAGCCGC
KK260	GCTATCAACGCGGCCGCTATTGGGCATAAGTATTAGGCGCATTTG
KK261	AACTAAATCGCGGCCTTTCAGAAAGATTCCACAAGGCACAAC
KK262	GTTCCTTGGGCGGCCTCCAAGGTGGTGTCTTCCAC
KK263	TGCACCATAGCGGCCGCATTGATCTTGGCCGCAAGAG
KK305	CCCGGGGTTGATAGCTTGGCGTAATCATG
KK312	CAAGCTATCAACCCCGGGATACTTGGGATTTACTTATTGGACTAACCC AG
KK313	CTTGCTCACCATCCCGCCTCGAAACGAGCGAAAGATC
KK314	AATCAATTGCCCCCCATCAGACGTTTAAAGTACCCACG
KK315	GAGTGCACCATACCCGGGACCGGAACGGTATAGTCTATGC
KK318	CCAGTAGCAACTTTATTATACATAGTTGATAATTCACTGGC
KK319	GATGCCATCTGTGGGGTTTATTGTTCAGAGAAG
KK320	CCCACAGATGGCATCCCTTAACCTTTCATC

KK321	TGTCCATCTTTCGAAGTTCTACATAATTTGCTGG
KK322	TTCGAAAGATGGACAACACCGAGGACGTCATC
KK323	TAAAGTTGCTACTGGGAGCCGGAGTGGC
KK346	ATGATGCGTCCCAAACCGGC
KK347	CTGTGGGGTTTATTGTTCAGAGAAGGGAG
KK348	CAATAAACCCCACAGATGGTGAGCAAGGGCGAGGAG
KK349	TTTGGGACGCATCATCTTGTACAGCTCGTCCATGCCGTG
RH140	TTTCAGGGACCCGGGATGATGCGTCCCAAACCGGC
RH142	TTCTTCTTCGTTGTTCTGTCCTTCGAAGTAGACGGCAGTC
RH143	AACAACGAAGAAGAAGCTTT
RH144	CCGTCTGTAAGTTGGACTAA
RH145	CCAACTTACAGACGGCTTCTCAGGCTCCGACATAA

RH146	GGCTTTGTTTAGCAGCTATCCACCTCTCTCGCCGA
RH150	ACGGGTGCCACGATGCTTGCGCGCGCG
RH151	CATCGTGGCACCCGTCCCTGGAGGTCC
RH152	GTGGACCAGATCGACTCACTATTGTCC
RH153	GTCGATCTGGTCCACAAAGATGATCGA
RH160	ATGGGTGTCGCCGATCTCATC
RH161	ATCGGCGACACCCATTGTTCTATCACACAAGGTGGGG
RH169	CTATCAACGCGGCCGCCCATTCTTTATGTTACTTCTATCCTG

RH170	GAACGGAACTAAATCCTTGACGGGTTTGTAGTGGAAG
RH171	AAGGATACTGTTCAGTCCGGAGGATCTGCGGGTGC
RH172	CGCAGATCCTCCGGACTGAACAGTATCCTTGGAGCC
RH173	GCTATCAACCCCGGGTATTGGGCATAAGTATTAGGCG
RH174	CTCATCGTCACCCCATATTGATCTTGGCCGCAAGAG
SH21	TATGGTGCACTCTCAGTACAATCTGC
SH22	TATGCGGTGTGAAATACCGCACAG
YHK196	CGTCGAGTCCACTGGTGTCTT
YHK197	TTGTTGACACCCATAACGAACATGG

YHK2 51	ATCAAGAAGTTCGAGTCCATCTCCAAGGTGGTGATGGTGAGCAAGGGCGAGGAG
YHK2 52	CTCGAACTTCTTGATGAGATCGGCGACACCCATCTGTGGGGTTTATTGTTCAGAGAAGGG
YHK2 55	GCTGCAACTACCTCGAACAACC
YHK2 56	TTGTCGCTCAACGCATCTTCAC
YM16	ATTTCACACCGCATAGGGGATCTGTAGTAGCTCGTGA
YM17	TGAGAGTGCACCATACGCTTAACAAGTATGATCGTCT
YM56	GATAACAATTTCACATATTGACTACTATGGTAACCAACGCG
YM60	TGTGAAATTGTTATCCGCTGGTATCAG
YM83	GCGGCCGCGTTGATAGCTTGGCG
pET50 b inf Fw	CTGCTAAACAAAGCCCGAAAGGAAGC

pET50

b inf　　CCCGGGTCCCTGAAAGAGGACTTCAAG

Rv

619

620 **Figure legends**

621 **Fig 1 Localization and endocytosis of AoCan1-EGFP in the Δ*aipA* strain.**

622 (A) The images of representative hyphae of each strain were taken by confocal

623 microscopy at 0, 30, 60, 90 min after the medium shift. Scale bar = 10 μm.

624 (B) The ratio of hyphae with AoCan1-EGFP endocytosed was measured at ten time

625 points for each strain. The error bars represent the SDs from three independent

626 experiments, each with n = 50. *, **Statistically significant difference at P < 0.05, 0.01,

627 respectively (Student's t test). a, b, c: Statistically significant difference at α = 0.05

628 (tukey-kramer's multiple test).

629

630 **Fig 2 Localization and endocytosis of AoCan1-EGFP in the Δ*Aoabp1* strain.**

631 (A) The images of representative hyphae of each strain were taken by confocal

632 microscopy at 0, 30, 60, 90 min after the medium shift. Scale bar = 10 μm.

633 (B) The ratio of hyphae with AoCan1-EGFP endocytosed was measured at ten time

634 points for each strain. The error bars represent the SDs from three independent

635 experiments, each with n = 50. *, **Statistically significant difference at P < 0.05, 0.01,

636 respectively (Student's t test). a, b, c: Statistically significant difference at α = 0.05

637 (tukey-kramer's multiple test).

Fig 3 Localization of Lifeact-EGFP in *aipA* and *Aoabp1* deletion strains.

(A) 1.0×10^5 conidia of each strain in 100 μL of CD medium were cultured at 30°C for 20 h, and subsequently observed under fluorescence microscope. Scale bar = 10 μm. (B) Fluorescence intensity profiles of Lifeact-EGFP in each strain were taken at the cross section of 2 μm from the hyphal tip.

Fig 4 Localization of EGFP-AipA and AoAbp1-mDsRed in Δ*aipA* and Δ*Aoabp1* cells.

(A) The images of representative hyphae of each strain expressing EGFP-AipA or AoAbp1-mDsRed were taken by confocal microscopy. Note that EGFP-AipA was dispersed from the hyphal tip region in the Δ*Aoabp1* cells. (B) EGFP-AipA$^{\Delta346\text{-}370}$ exhibited cytoplasmic localization. (C) EGFP-AipA^{E542A} showed similar localization to EGFP-AipA; in contrast, EGFP-AipA^{E596Q} exhibited both apical and basal localization. Scale bar = 10 μm.

Fig 5 Localization and endocytosis of AoCan1-EGFP in the Δ*aipA*Δ*Aoabp1* strain.

(A) The images of representative hyphae of each strain were taken by fluorescent

656 microscopy at 0, 30, 60, 90 min after the medium shift. Scale bar = 10 μm.

657 (B) The ratio of hyphae with AoCan1-EGFP endocytosed was measured at ten time

658 points for each strain. The error bars represent the SDs from three independent

659 experiments, each with *n* = 50. *Statistically significant difference at *P* < 0.05 (Student's

660 *t* test).

661

662 **Fig 6 Localization and endocytosis of AoCan1-EGFP in *aipA*-, *aipA*^{K542A}- and**

663 ***aipA*^{E596Q}-overexpressing strains.**

664 (A) The images of representative hyphae of each strain were taken by confocal

665 microscopy at 0, 30, 60, 90 min after the medium shift. Scale bar = 10 μm.

666 (B) The ratio of hyphae with AoCan1-EGFP endocytosed was measured at ten time

667 points for each strain. The error bars represent the SDs from three independent

668 experiments, each with *n* = 50. a, b, c: Statistically significant difference at *α* = 0.05

669 (tukey-kramer's multiple test).

670

671 **Fig 7 Localization of EGFP-AipA in the *aipA*-overexpressing background.**

672 Hyphal images of each strain were taken by confocal microscopy at approximately 30

673 min after the treatment of NOC or its solvent DMSO. Scale bar = 10 μm.

674

675 **Fig 8 Localization and endocytosis of AoCan1-EGFP in *aipA*-, *aipA*^{K542A}-and**

676 ***aipA*^{E596Q}-complementary strains.**

677 (A) The images of representative hyphae of each strain were taken by confocal

678 microscopy at 0, 30, 60, 90 min after the medium shift. Scale bar = 10 μm.

679 (B) The ratio of hyphae with AoCan1-EGFP endocytosed was measured at ten time

680 points for each strain. The error bars represent the SDs from three independent

681 experiments, each with n = 50. a, b: Statistically significant difference at α = 0.05

682 (tukey-kramer's multiple test).

683

684 **Fig 9 Schematic diagram of AoCan1 endocytosis in *A. oryzae*.**

685 The rate of AoCan1 endocytosis is depicted as the width of the arrow (red, accelerated;

686 blue, delayed) in WT and each mutant strain.

Fig. 1 Hiasa et al.

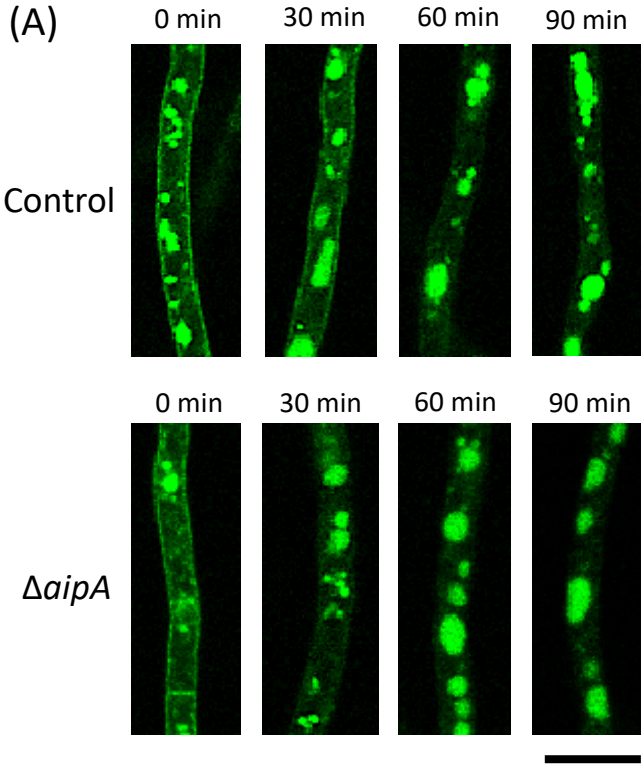

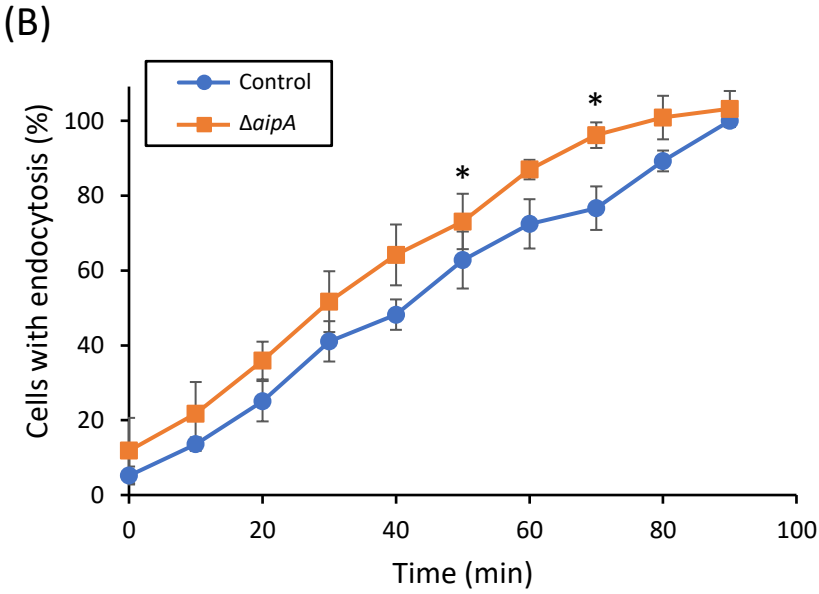

Fig. 2 Hiasa et al.

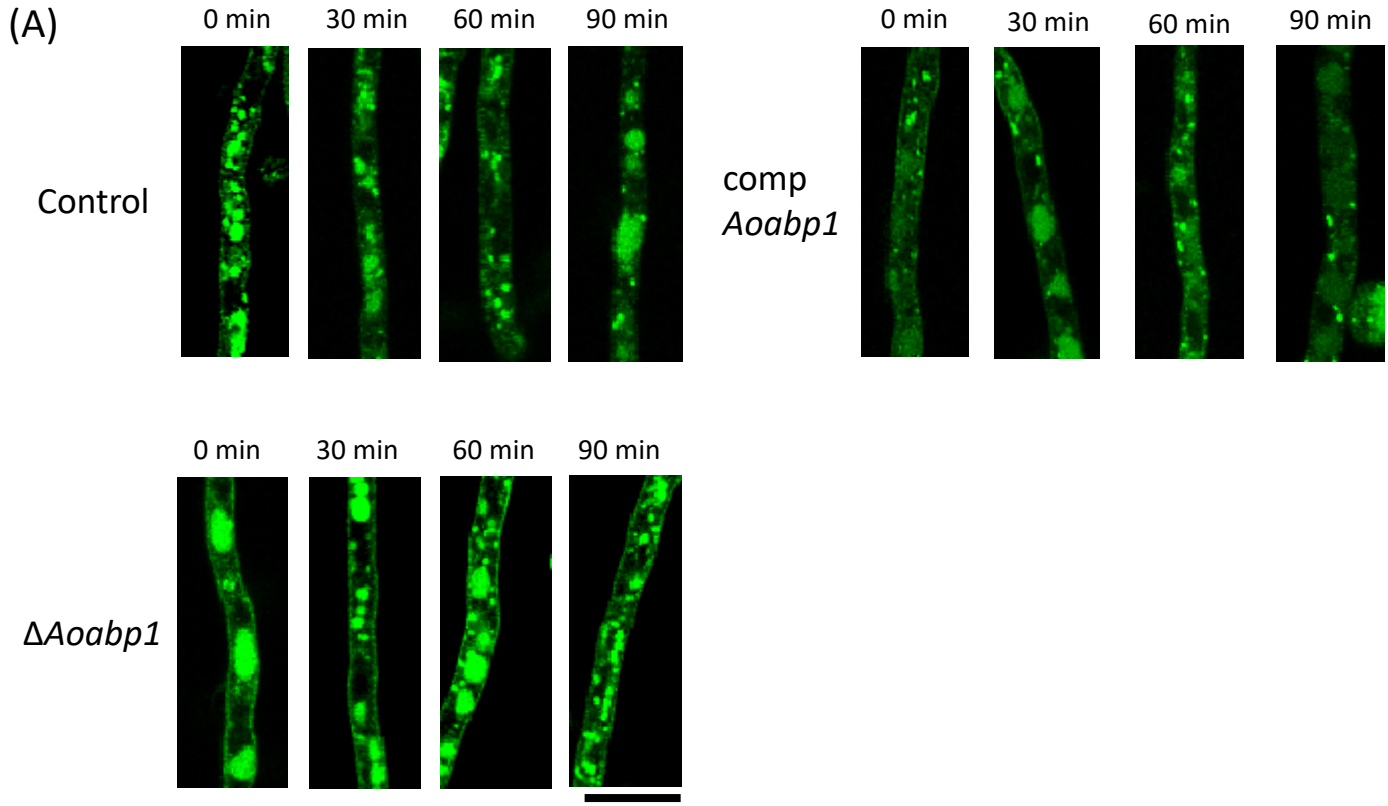

Fig. 3 Hiasa et al.

(A)

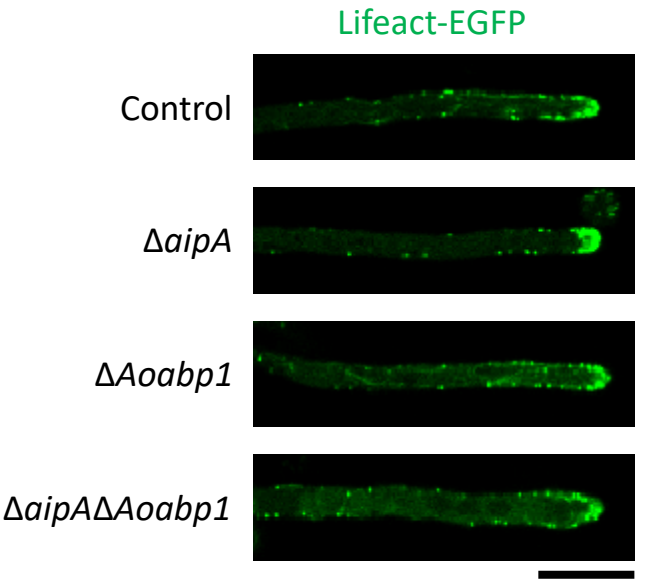

(B)

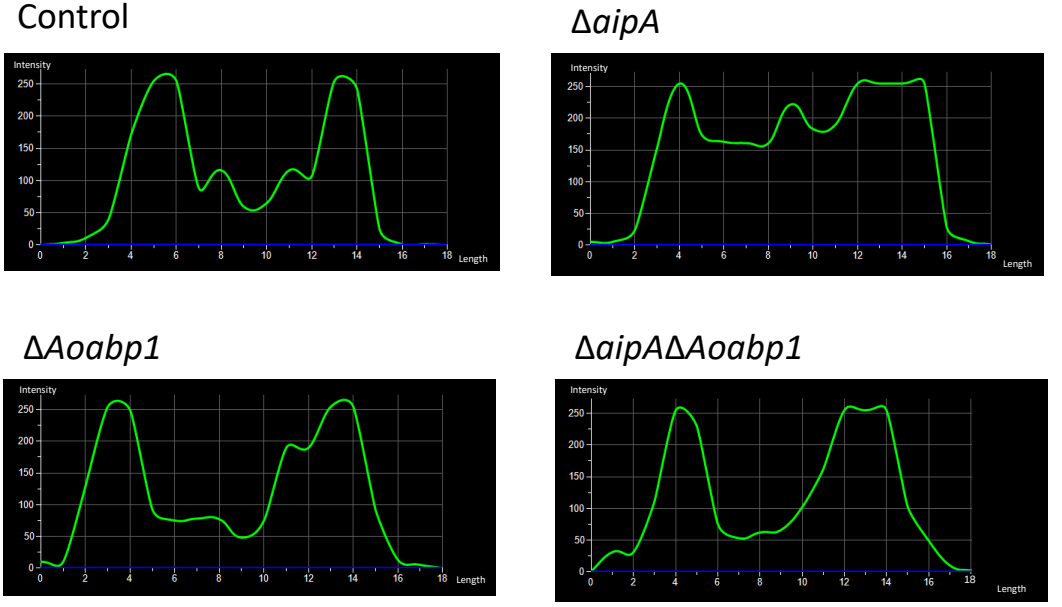

Fig. 4 Hiasa et al.

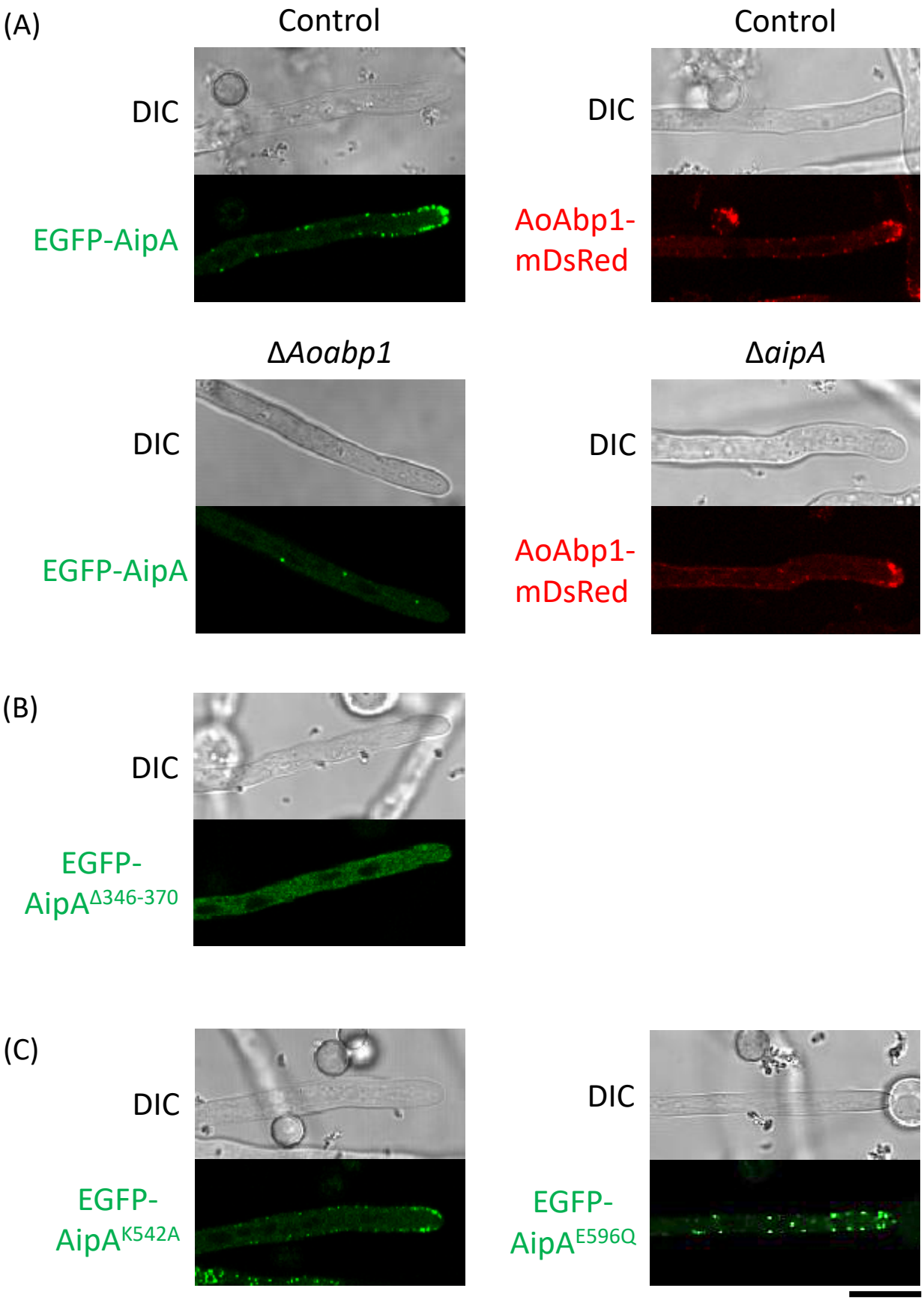

Fig. 5 Hiasa et al.

(A)

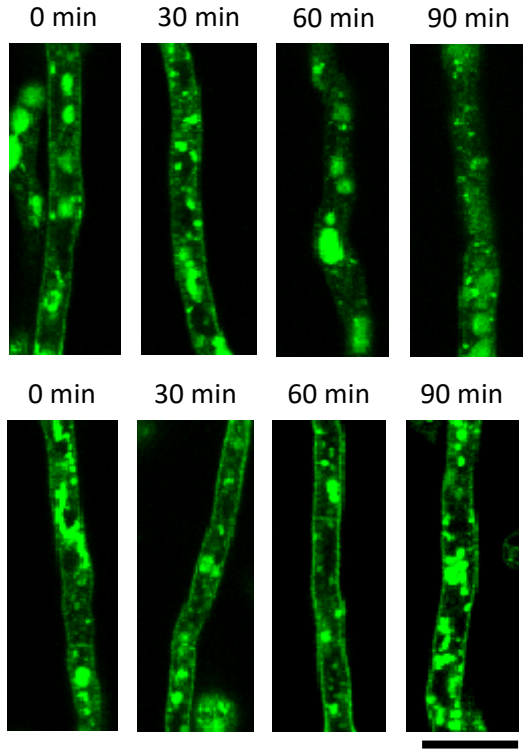

(B)

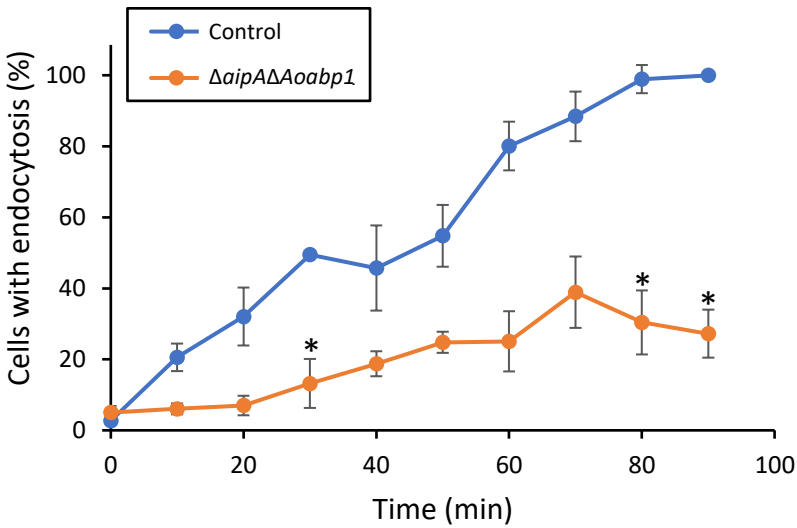

Fig. 6 Hiasa et al.

(A)

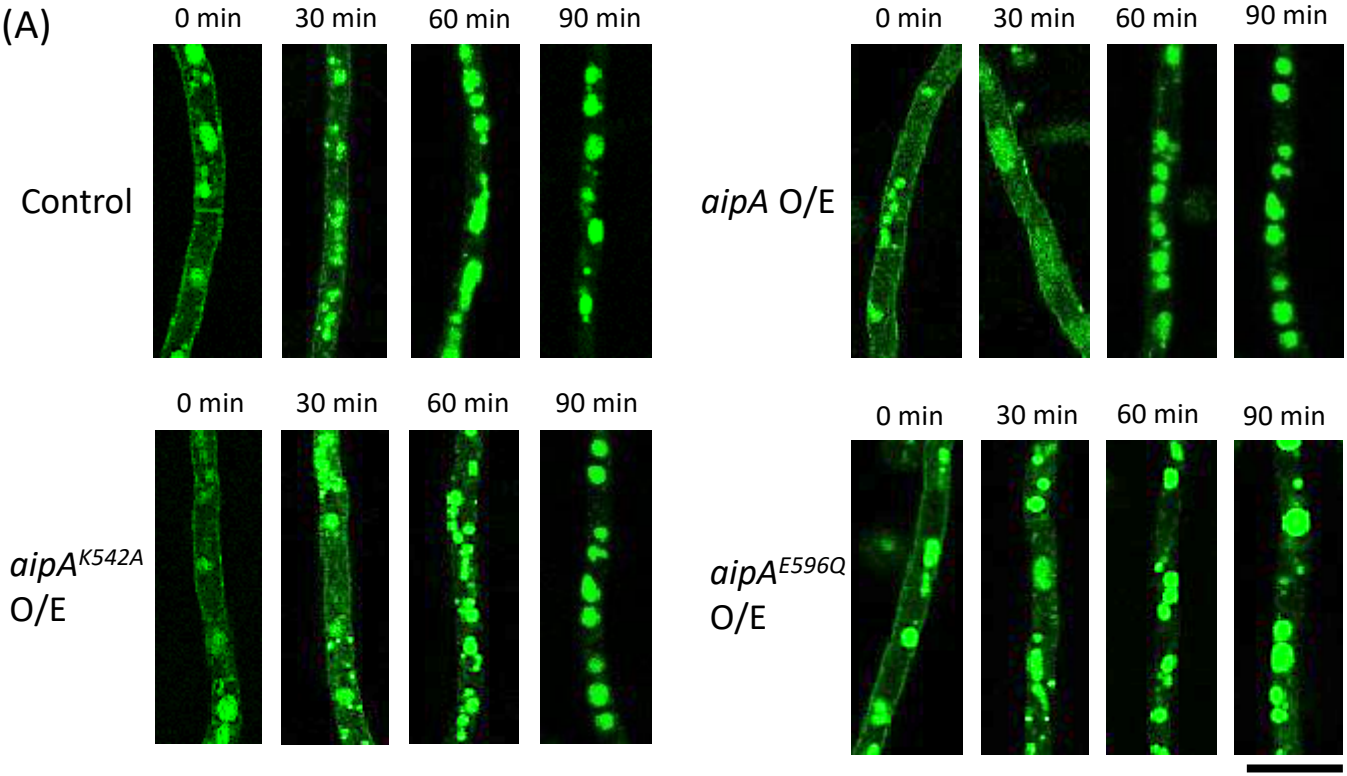

(B)

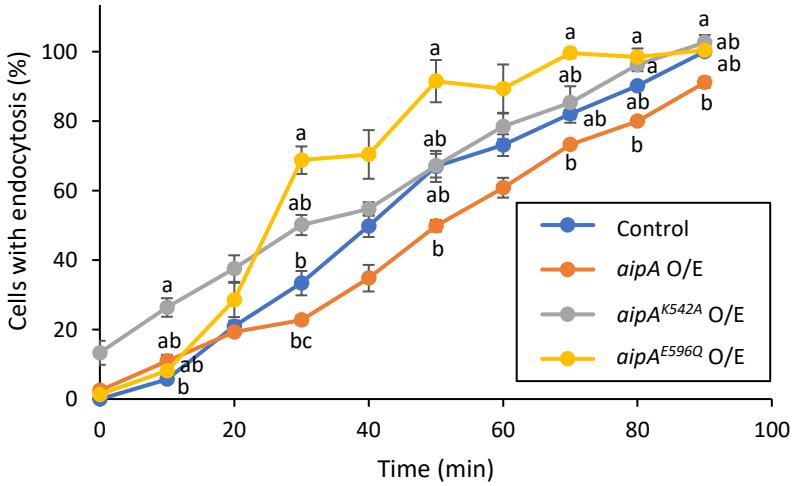

Fig. 7 Hiasa et al.

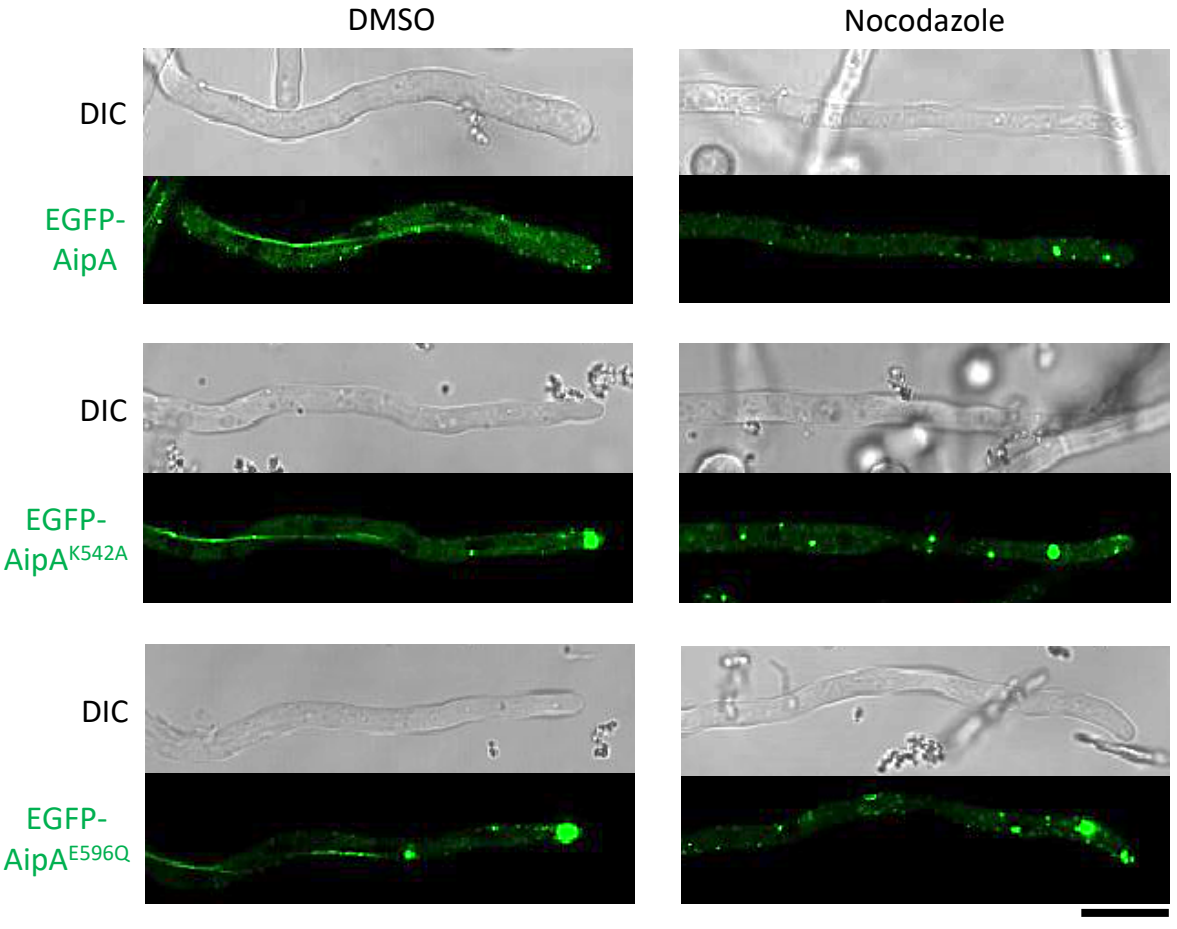

Fig. 8 Hiasa et al.

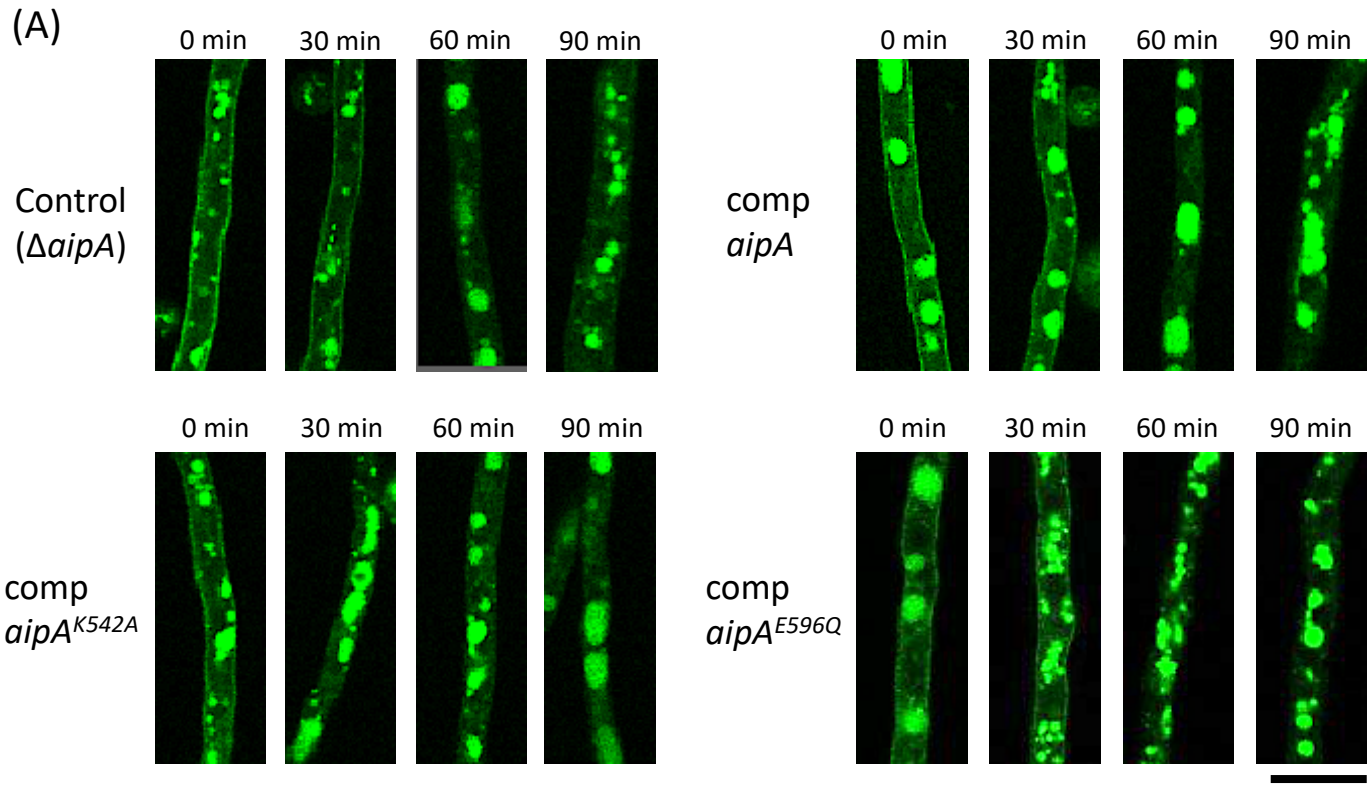

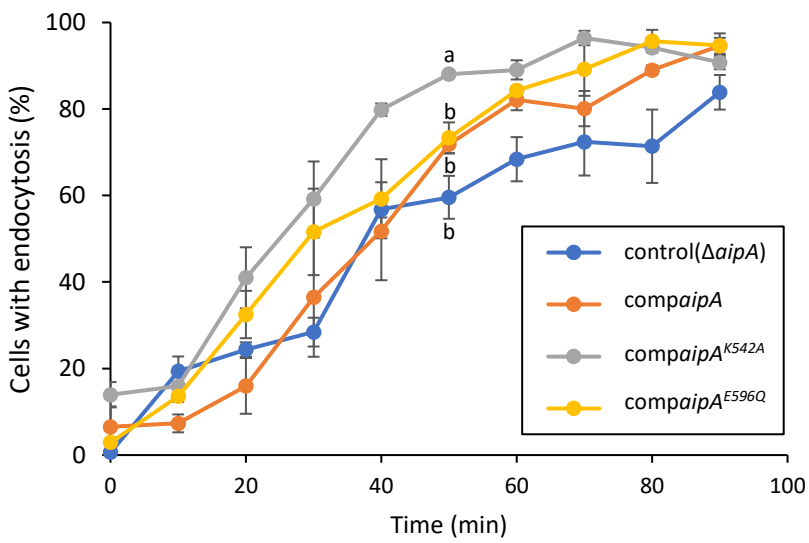

Fig. 9 Hiasa et al.

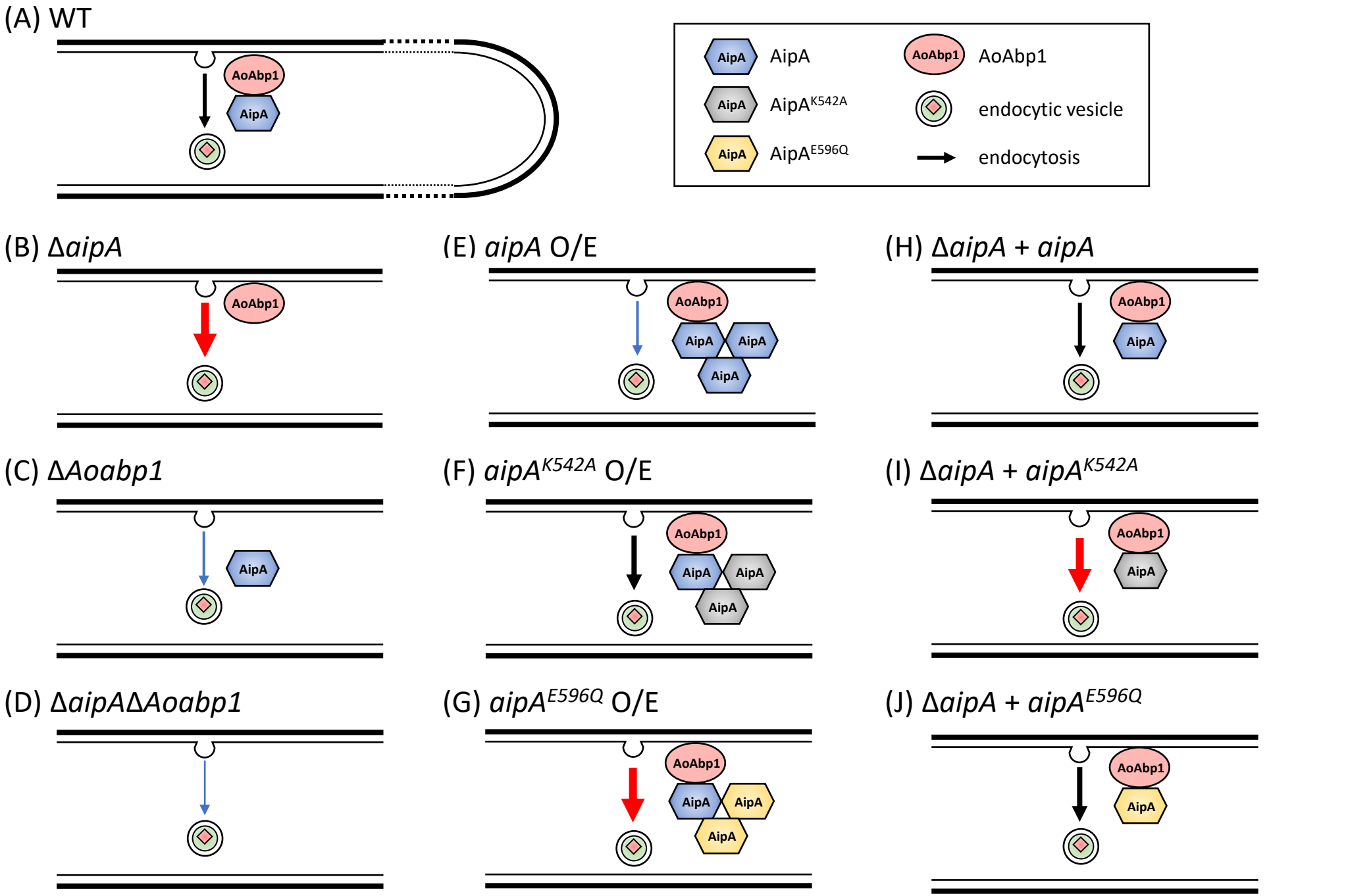

Supplementary materials

Involvement of AAA ATPase AipA in endocytosis of the arginine permease AoCan1 depending on AoAbp1 in *Aspergillus oryzae*

Reiko Hiasa, Ken-ichi Kakimoto, Kaoru Takegawa, Yujiro Higuchi*

Department of Bioscience and Biotechnology, Faculty of Agriculture, Kyushu University, 744 Motooka, Fukuoka 819-0395, Japan

*Corresponding author. Tel/Fax: +81 92 802 4734, E-mail address: y.higuchi@agr.kyushu-u.ac.jp

Word count: Abstract, 250; Main, 5519.

Number of figures: Main, 9; Supplementary, 5.

Number of tables: Main, 2.

Supplementary figure legends

Fig S1 Localization of EGFP-AoSnc1 in deletion strains.

Approximately 1.0×10^5 conidia of each strain in 100 μL of CD medium were cultured at 30°C for 20 h, and subsequently observed under confocal microscope. Scale bar = 10 μm.

Fig S2 Growth test of deletion strains.

Approximately 1.0×10^4 conidia of each strain were inoculated onto PD or M medium plate added with the indicated reagent, and were cultured at 30, 37°C for 4 days.

Fig S3 AAA ATPase assay of AipA.

AAA ATPase activity was measured using the recombinant AipA. The vertical axis is the relative ratio with the ATPase activity of WT=1. The error bars represent the SDs from three independent experiments, each with *n*=3.

Fig S4 Expression analysis of *aipA*-, *aipA*^{K542A}- and *aipA*^{E596Q}-overexpressing strains.

Relative expression levels of *aipA* in cells of each strain cultured with maltose,

normalized by the expression of *gpdA*. The relative ratios are depicted with the expression level of the control strain as 1. The error bars represent the SDs from three independent experiments, each with *n*=3.

Fig S5 Expression analysis of *aipA*-, *aipA*^{K542A}- and *aipA*^{E596Q}-complementary strains.

Relative expression levels of *aipA* in cells of each strain cultured in CD medium, normalized by the expression of *gpdA*. The relative ratios are depicted with the expression level of the *aipA*-complementary strain as 1. The error bars represent the SDs from three independent experiments, each with *n*=3.

Fig. S1 Hiasa et al.

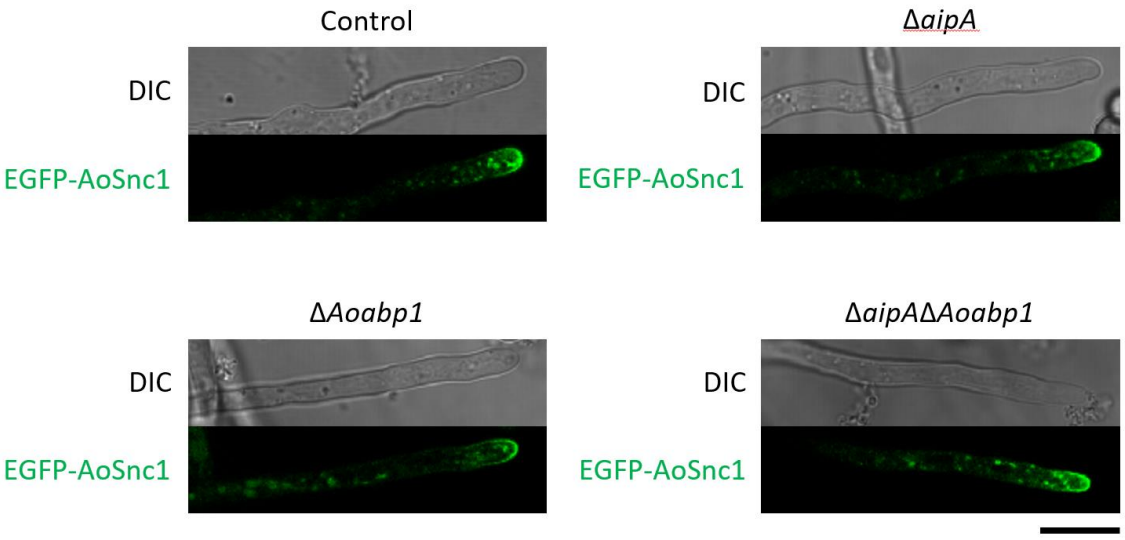

44

Fig. S2 Hiasa et al.

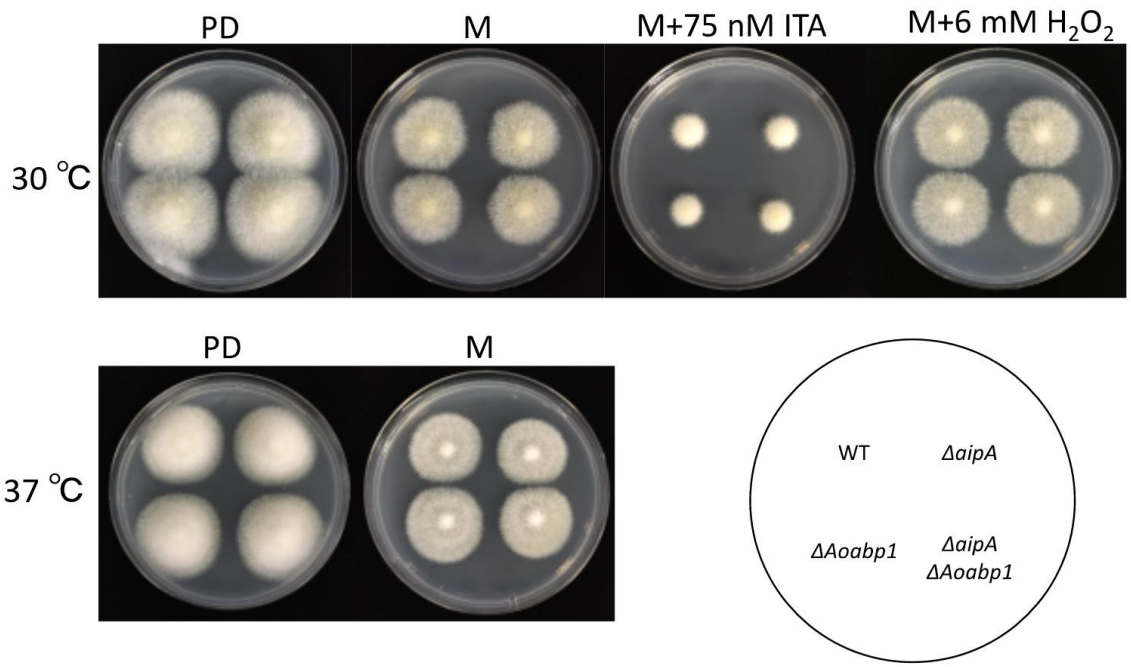

45

Fig. S3 Hiasa et al.

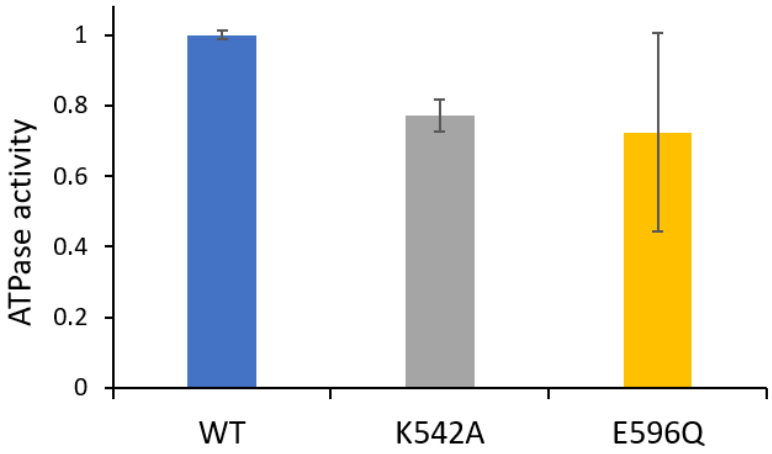

46

Fig. S4 Hiasa et al.

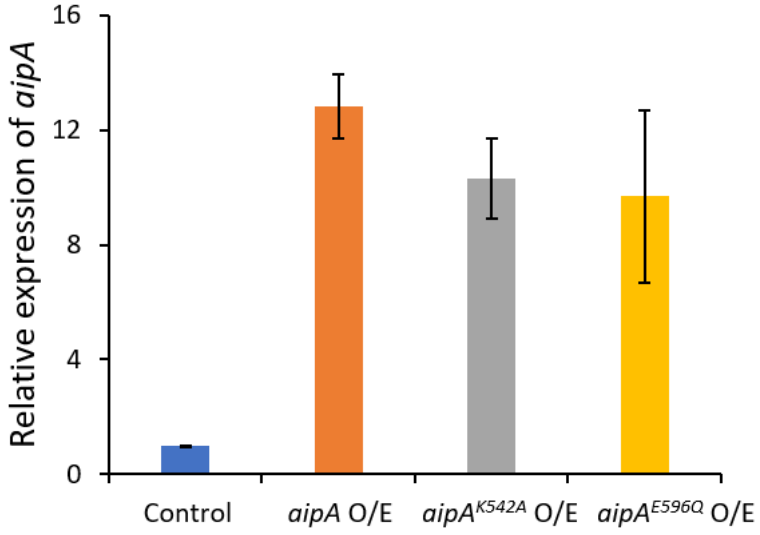

47

Fig. S5 Hiasa et al.

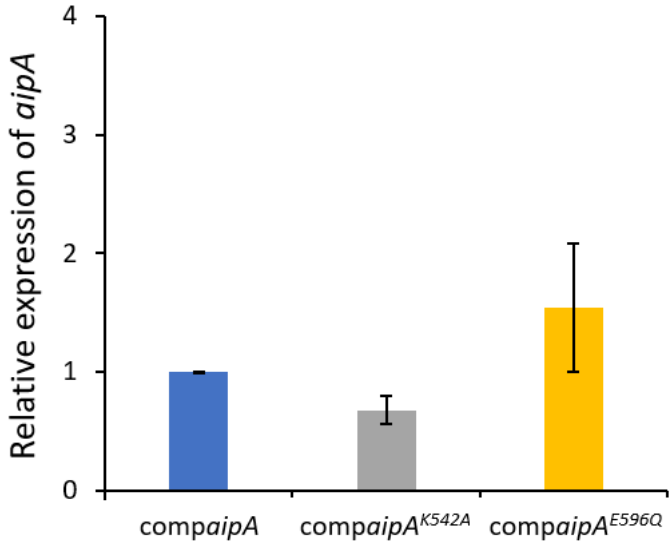

48